Resummation predictions for new electroweak gauge boson production at the LHC

Resummationsvorhersagen für die Produktion neuer elektroschwacher Eichbosonen am LHC

David Regalado Lamprea

Master's Thesis

presented at

Institut für Theoretische Physik
Westfälische Wilhelms-Universität Münster

in partial fulfilment of the requirements for the degree of

Master of Science

Supervisor · *Erstgutachter*: Prof. Dr. Michael Klasen
Westfälische Wilhelms-Universität Münster
Examiner · *Zweitgutachter*: Prof. Dr. Juan Antonio Caballero Carretero
Universidad de Sevilla

A la memoria de mi madre.

Zur Erinnerung an meine Mutter.

To the memory of my mother.

Contents

Chapter 1

Introduction

'Beauty is truth, truth beauty, — that is all
Ye know on earth, and all ye need to know.'
— John Keats in *Ode on a Grecian Urn.*

Mathematically speaking, precision makes a quantitative difference. A few more digits in a mathematical quantity mean just a better approximation. But in physics, precision makes indeed a qualitative difference, for a higher accuracy in the theoretical computation of a quantity may completely rule out a whole theory when accompanied by precise enough experimental data. And there is now a huge source of high-precision experimental results, namely the Large Hadron Collider (LHC) at CERN.

Due to the hadronic nature of the LHC and its high working energy, perturbative QCD is a cornerstone in the computational framework used by theorists around the world, and developments in the field are of crucial importance. In this context comes the importance of the resummation procedure, which is an improvement over fixed-order perturbative QCD in kinematical regions where these computations become unreliable, because of the appeareance of potentially large logarithms in the perturbative series that appear together with the strong coupling, spoiling its convergence near certain kinematical points. Resummation takes advantage of the definite structure of these logarithms to resum them to all orders, restoring the convergence properties of the series and overall improving the precision of the computations.

With the recent discovery of (a particle compatible with) the Higgs boson [1, 2] which closes the SM of particle physics, it is now needed to look for theories Beyond the Standard Model (BSM). From the many different possibilities, supersymmetric models are a very promising candidate for BSM physics, at least from a theoretical point of view. Many other promising candidates are related to the modification of the SM gauge groups either from a Grand Unified Theory (GUT) point of view (superstring-inspired or

not) or from specific models that address particular issues, like the models which restore the left-right symmetry to the SM. These models have very interesting theoretical consequences, e.g. some lead to force unification, as well as phenomenological ones, e.g. some require the appearance of right-handed neutrinos. One of the properties of these theories is that they all include new gauge bosons Z' or W' associated with the new gauge groups. Resummation procedures have long been applied sucessfully to Standard Model (SM) computations (e.g., Ref. [3]), and for BSM theories, to many supersymmetric particles [4, 5, 6, 7, 8, 9, 10]. However, only one example of resummation for a specific Z'-model exists [11], and no resummation computations have been applied to W' production yet. As the center-of-mass energy at the LHC increases and no BSM particles are found, it is necessary to perform more accurate predictions for a wider range of theories, like those including new gauge bosons. This will be the aim of this work.

In Ch. 2 we will review the basic concepts of the physics of hadron colliders. In Ch. 3 we will present the necessary formulae for the application of threshold and transverse momentum resummation formalisms. In Ch. 4 we will review the most important theories which include new gauge bosons and will study their phenomenology. In Ch. 5 we compute the fixed-order cross sections at NLO for new gauge boson production at the LHC, which needs to be matched with the resummation results. In Ch. 6 we will show and analyze numerical results performed for a few chosen benchmark points for different models of those previously presented. Our conclusions will be presented in Ch. 7 and resummation results for gaugino production in App. A.

Chapter 2

Physics of hadron colliders

We are, I think, in the Road of Improvement, for we are making Experiments.
— Benjamin Franklin in a letter to Jonathan Shipley.

In this chapter we will present a brief review of the canonical Drell-Yan process as an introduction to the physics of hadron colliders. This process will serve as the basis for the rest of this work and we will take the opportunity to fix some notations and discuss some useful variables and the concept of parton distribution function (PDF).

2.1 Introduction to the Drell-Yan process

The paradigm process in hadron-hadron (in particular proton-proton) collisions is arguably the production of a lepton pair via a vector boson channel

$$pp \to \gamma, Z \to l^+ l^- + X, \tag{2.1}$$

the so-called Drell-Yan process (see Fig. 2.1). It is one of the simplest final states that can be produced in a hadron collider and includes all the features of a typical hadronic process.

Hadrons are not elementary particles, but are composed of quarks and gluons (partons), that interact under Quantum Chromodynamics (QCD). In QCD, the strong coupling α_S is scale-dependent and because of the property of asymptotic freedom, the strong coupling vanishes for asymptotically large scales like the ones in a collider as the LHC. The behaviour under a scale $\mu \to \infty$ is

$$g(\mu) \sim 1/\log\left(\frac{\mu}{\Lambda}\right), \tag{2.2}$$

where Λ is the strong interaction scale. Thus, it may seem reasonable to attempt a perturbative approach for a high enough energy scale μ. However, in the computation of an n-th order correction, the couplings appear in the

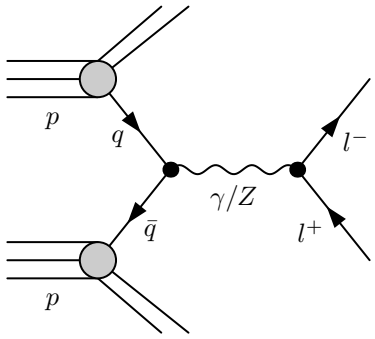

Figure 2.1: Drell-Yan process at leading order.

combination $g^{2n}(\mu)\log^{kn}(\mu/m)$, where $k \in \{1,2\}$ and m is a typical mass scale, thus spoiling the convergence of the series when $\mu \ll m$. This means that the contribution from long-distance physics enters crucially in the cross section computation, while only small-distance physics can be computed perturbatively. It turns out, however, that both scales can be separated thanks to the QCD factorization theorem[1] using the *parton distribution functions* (PDFs). We will review here these concepts in application to the Drell-Yan process.

2.2 Parton distribution functions

In hadron colliders, the fact that hadrons are not elementary particles leads to a phenomenological difficulty: the theoretical cross sections depend on the energy of the elementary components of the hadrons, while experimentally only the hadron energy is known. It is therefore necessary to work with the energy distribution of the partons inside the hadron to make useful predictions. If we assume that there is no transversal momentum for the partons inside the hadron, $p_{\mathrm{T}}^a = 0$, we can define the probability of the parton a inside a hadron A having a fraction x of its momentum as the parton distribution function $f_{a/A}(x)$, where a represents the different partons inside the hadron, most importantly u, d, c, s, g, which are assumed to be massless, and A will be implicitly the proton except otherwise noted, since we are focusing on the LHC.

The different $f_{a/A}(x)$ functions are not independent from each other [13]. By using CP symmetry (exact in QCD), proton and anti-proton PDFs can be related by $f_q^{\bar{p}}(x) = f_{\bar{q}}(x)$, $f_{\bar{q}}^{\bar{p}}(x) = f_q(x)$ and $f_g^{\bar{p}}(x) = f_g(x)$ for all $x \in [0,1]$. In the case of the proton, the expectation value for the valence quarks is

[1] For a review, see e.g. Ref. [12].

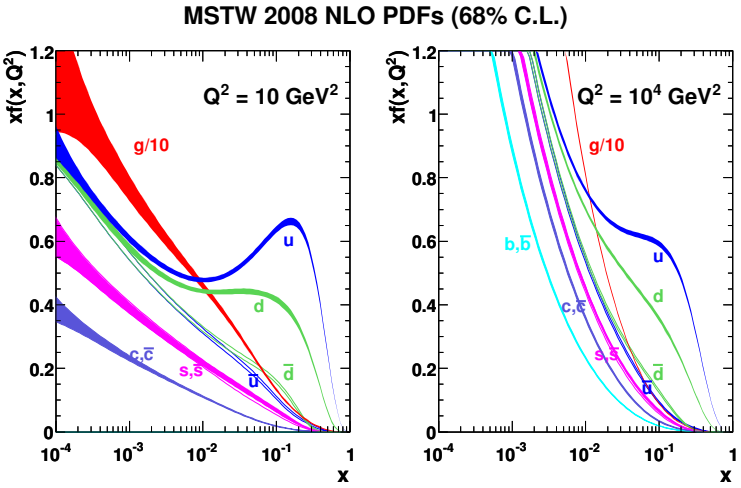

Figure 2.2: Plots of the x-dependence of the MSTW 2008 PDF at next-to-leading-oder for the different partons inside a proton at energies of $Q^2 = 10$ GeV^2 and $Q^2 = 10^4$ GeV^2.

trivially

$$\langle N_u \rangle = \int_0^1 \mathrm{d}x (f_u(x) - f_{\bar{u}}(x)) = 2, \quad \langle N_d \rangle = \int_0^1 \mathrm{d}x (f_u(x) - f_{\bar{u}}(x)) = 1, \tag{2.3}$$

and the the different contributions from the different partons are related by

$$\langle \sum x_i \rangle = \int_0^1 \left(\sum_q f_q(x) + \sum_{\bar{q}} f_{\bar{q}}(x) + f_g(x) \right) x \mathrm{d}x = 1. \tag{2.4}$$

Parton distribution functions cannot be computed theoretically, but they are universal for every process and their evolution is known to obey the DGLAP equation for their energy-dependence, which they acquire after renormalization (see next section), so they can be measured in one experiment and used in different processes at different energies. The x-dependence cannot be predicted theoretically, so this dependence is parametrized and fitted at different energies by using Deep Inelastic Scattering (DIS) data. The results of this parametrization obtained by the MSTW group [14] are shown in Fig. 2.2, which will be the ones used in this work.

2.3 QCD factorization and divergences

Drell and Yan [15] proposed in 1970 to use the parton model developed for Deep Inelastic Scattering (DIS) to the process in Eq. (2.1). At leading order,

the hadronic cross section can be naïvely expressed as the convolution of the partonic cross section $\hat{\sigma}$ for $q\bar{q} \to \gamma, Z \to l^+l^-$, with the parton distribution function of a parton i inside the proton at a fraction of the momentum x, $f_i(x)$

$$\sigma = \sum_{i,j} \iint \mathrm{d}x_1 \mathrm{d}x_2 \, f_i(x_1) f_j(x_2) \, \hat{\sigma}_{i,j}. \tag{2.5}$$

Formally this is valid in the limit $M^2, s \to \infty,\ \tau := M^2/s$ fixed. This theoretical assumption has proven to give successful predictions when compared to the experiments [16].

Equation (2.5) can be applied to leading-order (LO) cross sections giving finite results. However, when computing next-to-leading (NLO) corrections to the partonic cross section it is found that two types of divergences appear. First, the usual ultraviolet divergences, which are isolated using dimensional regularization and cancelled by including the appropriate counter-terms in the Feynman rules. This introduces a new dependency on the renormalization scale μ_R [17]. We will now briefly discuss the other type of divergences, the infrared divergences and their relation to the PDFs.

If we consider that for example, a gluon with momentum k is emitted from the incoming quark with momentum p_a and working in the massless quark limit, we find that the matrix element will contain a term of the form

$$\frac{1}{(p_a - k)^2} = \frac{1}{-2|p_a||k|(1 - \cos\theta)}, \tag{2.6}$$

where θ is the angle between the two momenta. We can see that there exists a divergence in the case that $|k| \to 0$ (*soft* divergence) or when $\cos\theta \to 1$ (*collinear* divergence). It can be proven that the short-distance physics (finite) and the long-distance physics (divergent) factorize in the form

$$\hat{\sigma}_{i,j}(s) = \iint \mathrm{d}z_1 \mathrm{d}z_2 \Gamma_{i,k}(z_1, \mu_\mathrm{F}) \bar{\sigma}_{k,l}(z_1 z_2 s) \Gamma_{j,l}(z_2, \mu_\mathrm{F}), \tag{2.7}$$

where $z_i \in [0, 1]$ is the momentum fraction in the quark propagator (after some possible gluon emission) and $\Gamma_{i,j}$ is the parton-in-parton distribution and includes all the singularities. We also define the renormalized PDFs as

$$\bar{f} := \int_0^1 \mathrm{d}x \int_0^1 \mathrm{d}z f(x) \Gamma(z, \mu_\mathrm{F}) \delta(\eta - xz) = \int_\eta^1 \mathrm{d}z \frac{1}{z} f\left(\frac{\eta}{z}\right) \Gamma(z, \mu_\mathrm{F}). \tag{2.8}$$

With these definitions it is easy to see that the hadronic cross section can be computed using only renormalized (finite) quantities,

$$\begin{aligned} \sigma_{A,B} &= \sum_{i,j} \iint \mathrm{d}x_1 \mathrm{d}x_2 \, f_i(x_1) f_j(x_2) \, \hat{\sigma}_{i,j} \\ &= \sum_{k,l} \iint \mathrm{d}\eta_1 \mathrm{d}\eta_2 \, \bar{f}_{k/A}(\eta_1) \bar{f}_{l/B}(\eta_2) \, \bar{\sigma}_{k,l}(\eta_1 \eta_2 s) \end{aligned} \tag{2.9}$$

We have introduced in the expressions the necessary factorization scale $\mu_{\rm F}$, which together with the renormalization scale $\mu_{\rm R}$, introduced to cancel ultraviolet divergences must be introduced also into Eq. (2.5), giving the final factorized form for the hadronic cross section,

$$\sigma(\mu_{\rm F},\mu_{\rm R}) = \sum_{i,j} \iint {\rm d}x_1 {\rm d}x_2\, \bar{f}_i(x_1,\mu_{\rm F}) \bar{f}_j(x_2,\mu_{\rm F})\, \bar{\sigma}_{i,j}(x_1x_2S, \alpha_S(\mu_{\rm R}^2), \mu_{\rm F}, \mu_{\rm R}). \tag{2.10}$$

From now on we will always use renormalized quantities except otherwise noted and will change the notation, dropping the bar over symbols for simplicity.

2.4 Kinematical variables

Kinematics in hadron colliders are special in the sense that the longitudinal momenta of the initial state partons for a given event are unknown, and must be then convoluted with the parton distribution functions. The kinematic variables used are therefore chosen according to this property to transform properly under longitudinal boosts.

We first try to substitute the variables x_1 and x_2 for more physical variables which transform easily under longitudinal boosts. A longitudinal boost from the rest frame can be expressed as

$$\begin{pmatrix} E \\ p_{\rm L} \end{pmatrix} = \exp\left[y \begin{pmatrix} 0 & 1 \\ 1 & 0 \end{pmatrix} \right] \begin{pmatrix} m \\ 0 \end{pmatrix} = m \begin{pmatrix} \cosh y \\ \sinh y \end{pmatrix}, \tag{2.11}$$

where we can see that two consecutive longitudinal boosts with parameters y_1 and y_2 are equivalent to a longitudinal boost of parameter $y = y_1 + y_2$. The parameter y is called the *rapidity,* and a somewhat more manageable but equivalent definition to that of Eq. (2.11) is

$$y := \frac{1}{2} \log \frac{E + p_{\rm L}}{E - p_{\rm L}}. \tag{2.12}$$

If we use the trivial relation $q^2 = x_1x_2S$, where q is the invariant mass of the gauge boson, and $\sqrt{S}$ is the hadronic center-of-mass energy, we obtain the following transformation,

$$x_1 = \sqrt{\frac{q^2}{S}} e^{y}, \qquad x_2 = \sqrt{\frac{q^2}{S}} e^{-y}. \tag{2.13}$$

In the massless limit, the expression for rapidity can be further simplified using $E = |\vec{p}|$, what leads to

$$\lim_{m\to 0} y = \frac{1}{2} \log \frac{E + p_{\rm L}}{E - p_{\rm L}} = \frac{1}{2} \log \frac{|\vec{p}| + p_{\rm L}}{|\vec{p}| - p_{\rm L}} = \frac{1}{2} \log \frac{1+\cos\theta}{1-\cos\theta} = -\log\tan\frac{\theta}{2} =: \eta, \tag{2.14}$$

where θ is the angle of the 3-momentum with respect to the beam direction and η is *the pseudo-rapidity*. In the massless case the pseudo-rapidity coincides with the rapidity, and in some other cases can be considered an approximation.

Other useful definitions which are trivially invariant under longitudinal boosts are the *transverse momentum* p_{T} and the *tranverse energy* E_{T}. If the 4-momentum is expressed as (E, p_x, p_y, p_z), then the transverse momentum is defined as

$$p_{\mathrm{T}} := \sqrt{p_x^2 + p_y^2}, \tag{2.15}$$

and the transverse energy is defined as

$$E_{\mathrm{T}} := \sqrt{p_x^2 + p_y^2 + m^2} = \sqrt{p_{\mathrm{T}}^2 + m^2}. \tag{2.16}$$

Throughout the rest of this work we will extensively use the transverse momentum p_{T}, as it is a crucial variable in the production of vector bosons in general, and when taking into account resummation in particular (see transverse momentum p_{T} resummation in Sec. 3.3).

When dealing with vector bosons decaying into two leptons, it is also useful to define the *invariant mass* M of the two outgoing particles by

$$\begin{aligned} M &:= \sqrt{(p_1^\mu + p_2^\mu)(p_{1,\mu} + p_{2,\mu})} \\ &= \sqrt{m_1^2 + m_2^2 + 2(E_1 E_2 - \vec{p_1} \cdot \vec{p_2})} \end{aligned} \tag{2.17}$$

and when the vector boson decays into a lepton and a neutrino, which is not detected in the collider, experimentalists tend to use the *transverse mass*, defined in an obvious way,

$$\begin{aligned} M_{\mathrm{T}} &:= \sqrt{(p_{\mathrm{T},1}^\mu + p_{\mathrm{T},2}^\mu)(p_{\mathrm{T},1,\mu} + p_{\mathrm{T},2,\mu})} \\ &= \sqrt{m_1^2 + m_2^2 + 2(E_{\mathrm{T},1} E_{\mathrm{T},2} - \vec{p_{\mathrm{T},1}} \cdot \vec{p_{\mathrm{T},2}})}. \end{aligned} \tag{2.18}$$

Chapter 3

Resummation

Truth is rarely pure and never simple.
— Oscar Wilde in *The Importance of Being Earnest.*

In this chapter we will introduce the concept of resummation and the basic ideas and necessary formulae for the specific application of the threshold and transverse momentum formalisms. We will not attempt to present here a complete, exhaustive or formal study of the resummation theory, but only review the most important ideas behind it in a practical way. The reader is referred to, e.g., Refs. [18, 19] for more comprehensive reviews and to, e.g., Ref. [3] for a formal presentation of the theory. The developments in this chapter will also be based on the works of Debove [7, 8, 20] and Fuks [21, 22, 23].

3.1 Philosophy of resummation

Resummation constitutes an improvement over the fixed-order perturbative QCD computations in certain kinematical regions, in which perturbation theory is unreliable. This is achieved by summing to all orders some potentially large (logarithmic) terms in the perturbative series thanks to the definite structure that they present.

The Kinoshita-Lee-Nauenberg theorem [24, 25] guarantees under our conditions that infrared singularities of virtual and real contributions to next-to-leading order cancel with each other in fixed-order perturbation theory, making the cross section an infrared-safe quantity. However, in certain kinematical regions (e.g., at $z = 1$ or $p_{\mathrm{T}} = 0$) the cancellation of these divergences is constrained, leaving potentially large terms in the partonic cross section. This leads to logarithmic terms that may spoil the convergence properties of the series, but may be summed to all order in α_{S} using resummation mechanisms.

To illustrate the idea of resummation, let us consider an infrared-sensitive

quantity $R(M^2, m^2)$, which depends on two scales m, M, such that $m \ll M$. The idea of resummation is intimately linked to the concept of factorisation, and to begin we must first find an appropriate factorization of the quantity R (which may be a very complex step),

$$R(M^2, m^2) = H(M^2/\mu^2)S(m^2/\mu^2), \tag{3.1}$$

where the two scales are separated by the introduction of a factorisation scale μ. It is important to point out that this factorisation may not hold in the usual space (e.g., the x-space), but rather in a conjugate one (e.g., Mellin space).

From the dependencies of H and S we can write the evolution equations

$$\frac{\mathrm{d}H}{\mathrm{d}\log\mu^2} = -\frac{\mathrm{d}S}{\mathrm{d}\log\mu^2} = \gamma_{\mathrm{S}}(\mu^2). \tag{3.2}$$

Solving the previous equation we obtain

$$S(m^2/\mu^2) = S(1)\exp\left(-\int_{m^2}^{\mu^2}\frac{\mathrm{d}q^2}{q^2}\gamma_{\mathrm{S}}(q^2)\right), \tag{3.3}$$

and by choosing the scale $\mu = M$, we can rewrite $R(M^2, m^2)$ as

$$R(M^2, m^2) = H(1)S(1)\exp\left(-\int_{m^2}^{M^2}\frac{\mathrm{d}q^2}{q^2}\gamma_{\mathrm{S}}(q^2)\right). \tag{3.4}$$

We can see in Eq. (3.4) that we no longer have the potentially large ratios in the quantities H and S which appear in Eq. (3.1), and so they can now be computed reliably in perturbation theory. The exponential factor is called the *Sudakov form factor*, and computing the so-called anomalous dimension γ_{S} to a specific order in α_{S} resums to a given accuracy.

3.2 Threshold resummation

Threshold resummation attempts to resum the logarithmic terms of the form

$$a_{\mathrm{S}}^n\left(\frac{\log^m(1-z)}{(1-z)}\right)_+ \tag{3.5}$$

where $m \leq 2n-1$, which appear in the partonic cross section $\hat{\sigma}_{ab}$ in the limit $z := M^2/s \to 1$.

It is convenient to work in the Mellin space, defined by the Mellin transform

$$\tilde{F}(N) := \int_0^1 \mathrm{d}x\, x^{N-1}F(x). \tag{3.6}$$

As an abuse of notation, we will write the transformed quantities without tilde from now on, and just by changing the argument to the Mellin momentum N, i.e., $\tilde{F}(N) \equiv F(N)$.

Using this transformation we can rewrite the doubly differential hadronic cross section

$$M^2 \frac{\mathrm{d}^2\sigma_{AB}}{\mathrm{d}M^2\mathrm{d}p_\mathrm{T}^2}(\tau) = \sum_{ab} \int_0^1 \mathrm{d}x_a \int_0^1 \mathrm{d}x_b \, x_a f_{a/A}(x_a,\mu^2) x_b f_{b/B}(x_b,\mu^2) \times z\hat{\sigma}_{ab}(z, M^2, M^2/p_\mathrm{T}^2, M^2/\mu^2)\delta(\tau - x_a x_b z), \quad (3.7)$$

with $\tau := M^2/S$, as

$$M^2 \frac{\mathrm{d}\sigma_{AB}}{\mathrm{d}M^2\mathrm{d}p_\mathrm{T}^2}(N-1) = \sum_{ab} f_{a/A}(N,\mu^2) f_{b/B}(N,\mu^2) \times \hat{\sigma}_{ab}(N, M^2, M^2/p_\mathrm{T}^2, M^2/\mu^2). \quad (3.8)$$

The partonic cross section can also be expressed in a similar fashion

$$M^2 \frac{\mathrm{d}\sigma_{ab}}{\mathrm{d}M^2\mathrm{d}p_\mathrm{T}^2}(N-1) = \sum_{cd} \phi_{c/a}(N,\mu^2)\phi_{d/b}(N,\mu^2) \times \hat{\sigma}_{cd}(N, M^2, M^2/p_\mathrm{T}^2, M^2/\mu^2), \quad (3.9)$$

where $\phi_{c/a}(x_c,\mu^2)$ is the parton-in-parton distribution of parton c in parton d (similarly for $\phi_{d/c}$).

The evolution of the parton-in-parton distributions $\phi_{c/a}, \phi_{d/b}$ as a function of the scale is given by the Altarelli-Parisi equation [26],

$$\frac{\partial\phi_{c/a}(N,\mu^2)}{\partial \log\mu^2} = \sum_b P_{cb}(N, a_\mathrm{S}(\mu^2))\phi_{b/a}(N,\mu^2), \quad (3.10)$$

where P_{cb} are the splitting functions, which are calculable in perturbation theory. As an example we give the LO values,

$$P_{qq}^{(\mathrm{LO})}(N) = C_F\left(\frac{3}{2} + \frac{1}{N(N+1)} - 2\sum_{k=1}^{N}\frac{1}{k}\right), \quad (3.11)$$

$$P_{qg}^{(\mathrm{LO})}(N) = \frac{1}{2}\left(\frac{2+N+N^2}{N(N+1)(N+2)}\right), \quad (3.12)$$

$$P_{gq}^{(\mathrm{LO})}(N) = C_F\left(\frac{2+N+N^2}{N(N^2-1)}\right), \quad (3.13)$$

$$P_{gg}^{(\mathrm{LO})}(N) = \beta_0 + 2C_A\left(\frac{1}{N(N-1)} + \frac{1}{(N+1)(N+2)} - \sum_{k=1}^{N}\frac{1}{k}\right). \quad (3.14)$$

We can introduce the QCD evolution operator $E_{ab}(N, \mu^2, \mu_0^2)$ defined by

$$\frac{\partial E_{ab}(N, \mu^2, \mu_0^2)}{\partial \log \mu^2} = \sum_c P_{ac}(N, a_{\rm S}(\mu^2)) E_{cb}(N, \mu^2, \mu_0^2), \tag{3.15}$$

with which we can write the solution of the Altarelli-Parisi equation as

$$\phi_{c/a}(N, \mu^2) = \sum_b E_{cb}(N, \mu^2, \mu_0^2) \phi_{b/a}(N, \mu_0^2). \tag{3.16}$$

Applying the Mellin transform to the logarithmic term (3.5) we can see that

$$\left(\frac{\log^m (1-z)}{(1-z)} \right)_+ \to \log^{m+1} N + \cdots . \tag{3.17}$$

We will so-far retain only the leading terms in N, and especifically ignore contributions of $\mathcal{O}(1/n)$ in the splitting functions. In the limit $\log N \to \infty$ we can see that Eqs. (3.11)-(3.14) behave as

$$P_{qq}^{(\rm LO)}(N) = C_F \left(\frac{3}{2} - 2 \log \bar{N} \right) + \mathcal{O}\left(\frac{1}{N} \right), \tag{3.18}$$

$$P_{qg}^{(\rm LO)}(N) \sim \frac{1}{2N}, \tag{3.19}$$

$$P_{gq}^{(\rm LO)}(N) \sim \frac{C_F}{N}, \tag{3.20}$$

$$P_{gg}^{(\rm LO)}(N) = \beta_0 - 2 C_A \log \bar{N} + \mathcal{O}\left(\frac{1}{N} \right), \tag{3.21}$$

with $\bar{N} = N e^{\gamma_{\rm E}}$ and $\gamma_{\rm E}$ being the Euler constant.

From Eqs. (3.18)-(3.21) the mixing contributions can be ignored at leading power in N. Taking this into account and integrating Eq. (3.9) over $p_{\rm T}$, we arrive at

$$M^2 \frac{{\rm d}\sigma_{ab}}{{\rm d}M^2}(N-1) = \phi_{a/a}(N, \mu^2) \phi_{b/b}(N, \mu^2) \hat{\sigma}_{ab}(N, M^2, M^2/\mu^2) + \mathcal{O}\left(\frac{1}{N} \right). \tag{3.22}$$

Before resumming the logarithmic terms of the form in Eq. (3.5), it is necessary to factorise Eq. (3.22). Sterman [3] proved that the partonic cross section in Eq. (3.22) can be factorised in the form

$$M^2 \frac{{\rm d}\sigma_{ab}}{{\rm d}M^2}(N-1) = \psi_{a/a}(N, M^2) \psi_{b/b}(N, M^2) \times H_{ab}(M^2, M^2/\mu^2) S_{ab}(N, M^2/\mu^2) + \mathcal{O}\left(\frac{1}{N} \right). \tag{3.23}$$

The H_{ab} function is infrared-safe and does not depend on N, and thus can be computed perturbatively,

$$H_{ab}(M^2, M^2/\mu^2) = \sum_{n=0}^{\infty} a_{\rm S}^n H_{ab}^{(n)}(M^2, M^2/\mu^2), \tag{3.24}$$

the parton-in-parton distributions $\psi_{a/b}$ depend on invariant mass M instead of the scale μ and that satisfy the evolution equation

$$\frac{\partial \psi_{a/a}(N, M^2)}{\partial \log M^2} = \gamma_a(a_S(M^2))\psi_{a/a}(N, M^2), \tag{3.25}$$

being γ_a the anomalous dimension, which can also be computed perturbatively,

$$\gamma_a(a_S) = \frac{1}{Z_a}\frac{\partial Z_a}{\partial \log \mu^2} = \sum_n a_S \gamma_a^{(n)}, \tag{3.26}$$

and corresponds to the N-independent virtual terms in $P_{aa}(N, a_S)$. The function S_{ab} is related to the large-angle emission of soft-gluons and can be computed in the eikonal approximation.

From Eqs. (3.22) and (3.1) we obtain

$$\begin{aligned}\hat{\sigma}_{ab}(N, M^2, M^2/\mu^2) = &\frac{\psi_{a/a}(N, M^2)\psi_{b/b}(N, M^2)}{\phi_{a/a}(N, \mu^2)\phi_{b/b}(N, \mu^2)} \\ &\times S_{ab}(N, M^2/\mu^2)H_{ab}(M^2, M^2/\mu^2) + \mathcal{O}\left(\frac{1}{N}\right)\end{aligned} \tag{3.27}$$

It can be shown that by solving the evolutions equations for ϕ, ψ in the threshold limit and using gauge invariance and renormalisation group equations and the exponentiation of the eikonal function, the cross section can be expressed as

$$\hat{\sigma}_{ab}(N, M^2, M^2/\mu^2) = H_{ab}(M^2, M^2/\mu^2)\exp(G_{ab}(N, M^2, M^2/\mu^2)) + \mathcal{O}\left(\frac{1}{N}\right), \tag{3.28}$$

with

$$\begin{aligned}G_{ab}(N, M^2, M^2/\mu^2) = &\log \Delta_a(N, M^2, M^2/\mu^2) \\ &+ \log \Delta_b(N, M^2, M^2/\mu^2) \\ &+ \log \Delta_{ab}(N, M^2, M^2/\mu^2),\end{aligned} \tag{3.29}$$

where

$$\log \Delta_a(N, M^2, M^2/\mu^2) = \int_0^1 \mathrm{d}z\, \frac{z^{N-1} - 1}{1 - z} \int_{\mu^2}^{(1-z)^2 M^2} \frac{\mathrm{d}q^2}{q^2} A_a(a_S(q^2)), \tag{3.30}$$

$$\log \Delta_{ab}(N, M^2, M^2/\mu^2) = \int_0^1 \mathrm{d}z\, \frac{z^{N-1} - 1}{1 - z} D_{ab}(a_S((1 - z)^2 M^2)). \tag{3.31}$$

The collinear soft-gluon radiation from parton a is included in A_a, which is calculable perturbatively and D_{ab} contains the large-angle soft-gluon contributions and is also perturbatively calculable.

Integrating Eqs. (3.30) and (3.31) and inserting them into Eq. (3.4) we obtain

$$\hat{\sigma}_{ab}(N, M^2, M^2/\mu^2) = \mathcal{H}_{ab}(M^2, M^2/\mu^2) \times \exp(\mathcal{G}_{ab}(N, M^2, M^2/\mu^2)) + \mathcal{O}\left(\frac{1}{N}\right). \quad (3.32)$$

The difference between the hard function $\mathcal{H}_{ab}$ and H_{ab} is that the former includes the non-logarithmic terms wich result from the integrations,

$$\mathcal{H}_{ab}^{(0)}(M^2, M^2/\mu^2) = H_{ab}^{(0)}(M^2, M^2/\mu^2) \quad (3.33)$$

$$\mathcal{H}_{ab}^{(1)}(M^2, M^2/\mu^2) = H_{ab}^{(1)}(M^2, M^2/\mu^2) + \frac{\pi^2}{6}(A_a^{(1)} + A_b^{(1)})H_{ab}^{(0)}(M^2), \quad (3.34)$$

and $\mathcal{G}_{ab}$ can be shown to have the expansion

$$\mathcal{G}_{ab}(N, M^2, M^2/\mu^2) = \log \bar{N} g_{ab}^{(1)}(\lambda) + g_{ab}^{(1)}(\lambda, M^2/\mu^2) + a_S g_{ab}^{(3)}(\lambda, M^2/\mu^2) + \cdots \quad (3.35)$$

where $\lambda = a_S \beta_0 \log \bar{N}$. The functions $g_{ab}^{(i)}$ resum the logarithmic terms up to a given order. The term $g_{ab}^{(1)}$ is the leading logarithmic (LL) contribution and depends on $A_a^{(1)}$, while $g_{ab}^{(2)}$ depends on $A_a^{(1)}, A_a^{(2)}, D_{ab}^{(1)}$ and resums at the next-to-leading logarithmic (NLL) order. The rest of the $g_{ab}^{(i)}$ functions resum at higher orders.

We will now present the values of the functions for next-to-leading order (NLL) resummation. First, the $g_{ab}^{(i)}$ functions are [27]

$$2\lambda\beta_0 g_{ab}^{(1)}(\lambda) = (A_a^{(1)} + A_b^{(1)})(2\lambda + (1-2\lambda)\log(1-2\lambda) \quad (3.36)$$

$$\begin{aligned} 2\beta_0 g_{ab}^{(2)}(\lambda, M^2/\mu^2) = {} & (A_a^{(1)} + A_b^{(1)}) \log(1-2\lambda) \log \frac{M^2}{\mu^2} \\ & + (A_a^{(1)} + A_b^{(1)}) \frac{\beta_1}{\beta_0^2}(2\lambda + \log(1-2\lambda) + \frac{1}{2}\log^2(2-2\lambda)) \\ & - (A_a^{(1)} + A_b^{(1)}) \frac{1}{\beta_0}(2\lambda + \log(1-2\lambda)) + D_{ab}^{(1)} \log(1-2\lambda), \end{aligned} \quad (3.37)$$

with the coefficients

$$A_a^{(1)} = 2C_a, \quad (3.38)$$

$$A_a^{(2)} = 2C_a \left[\left(\frac{67}{18} - \frac{\pi^2}{6} \right) C_A - \frac{5}{9} n_f \right], \quad (3.39)$$

$$D_{ab}^{(1)} = 0, \quad (3.40)$$

where $C_q = C_F$ and $C_g = C_A$.

The $\mathcal{H}_{ab}$ function is, by comparing Eq. (3.32) with the perturbative expansion of $\hat{\sigma}_{ab}$, given by

$$\mathcal{H}_{ab}^{(0)}(M^2, M^2/\mu^2) = \hat{\sigma}_{ab}^{(0)}(M^2, M^2/\mu^2), \tag{3.41}$$

$$\mathcal{H}_{ab}^{(1)}(M^2, M^2/\mu^2) = \hat{\sigma}_{ab}^{(0)}(M^2, M^2/\mu^2) \tag{3.42}$$

$$\times (\mathcal{A}_0 + (\delta P_{aa}^{(1)} + \delta P_{bb}^{(1)}) \log \frac{M^2}{\mu^2} + \frac{\pi^2}{6}(A_a^{(1)} + A_b^{(1)})), \tag{3.43}$$

with $\delta P_{aa}^{(1)}$ the coefficient of the $\delta(1-x)$ term in the splitting function $P_{aa}^{(1)}$, and $\mathcal{A}_0$ is the infrared-finite part of the renormalised virtual correction, i.e.,

$$M^{\dagger(1)} M^{(0)} + \text{h.c.} = a_{\mathrm{S}} \left(\frac{4\pi\mu^2}{M^2}\right)^{\epsilon} \times \frac{\Gamma(1-\epsilon)}{\Gamma(1-2\epsilon)} \left(\frac{\mathcal{A}_{-2}}{\epsilon^2} + \frac{\mathcal{A}_{-1}}{\epsilon} + \mathcal{A}_0\right) |M^{(0)}|^2 + \mathcal{O}(\epsilon), \tag{3.44}$$

where the $\overline{\mathrm{MS}}$ renormalization scheme has been used.

The large logarithms must be resummed near the threshold, but the fixed-order predictions far from this threshold are still valid, so to obtain an expression valid for all kinematical regions it is necessary to do the *matching* of resummation predictions to fixed-order computations,

$$\hat{\sigma} = \hat{\sigma}_{\mathrm{res}} + \hat{\sigma}_{\mathrm{f.o.}} - \hat{\sigma}_{\mathrm{exp}}, \tag{3.45}$$

where $\hat{\sigma}_{\mathrm{res}}$ is the resummation cross section, $\hat{\sigma}_{\mathrm{f.o.}}$ is the fixed-order computations and $\hat{\sigma}_{\mathrm{exp}}$ is the result of the expansion of the resummed cross section to the same order in a_{S} as the perturbative result,

$$\hat{\sigma}_{ab}^{\mathrm{exp}} = H_{ab}^{(0)}(M^2, M^2/\mu^2) + a_{\mathrm{S}} H_{ab}^{(1)}(M^2, M^2/\mu^2)$$
$$-a_{\mathrm{S}} \left(2L - \log\frac{M^2}{\mu^2}\right) \sum_c (H_{ab}^{(0)}(M^2, M^2/\mu^2) P_{cb}^{(1)}(N) + P_{ca}^{(1)} H_{cb}^{(0)}(M^2, M^2/\mu^2))$$
$$- a_{\mathrm{S}} H_{ab}^{(0)}(M^2, M^2/\mu^2)(L^2(A_a^{(1)} + A_b^{(1)}) + L(B_a^{(1)} + B_b^{(1)})). \tag{3.46}$$

3.3 Transverse momentum (p_{T}) resummation

Transverse momentum resummation resums logarithms of the form

$$a_{\mathrm{S}}^n \left(\frac{\log^m(M^2/p_{\mathrm{T}}^2)}{p_{\mathrm{T}}^2}\right)_+, \tag{3.47}$$

where $m \leq 2n-1$, that appear in the transverse momentum distributions. We will now present the necessary formulae for this resummation in the Collins-Soper-terman (CSS) [28] formalism.

It is convenient in this case to work with the Fourier transform W_{ab} of cross section in Eq. (3.7),

$$M^2 \frac{\mathrm{d}^2\sigma_{ab}}{\mathrm{d}M^2 \mathrm{d}p_{\mathrm{T}}^2}(N) = \int \frac{\mathrm{d}^2}{4\pi} e^{i\mathbf{b}\cdot\mathbf{p}_{\mathrm{T}}} W_{ab}(N+1, M^2, M^2\bar{b}^2, M^2/\mu^2), \quad (3.48)$$

with b is the so-called *impact parameter* and $\bar{b} := b\gamma_{\mathrm{E}}/2$. The angular integration can be performed, yielding

$$M^2 \frac{\mathrm{d}^2\sigma_{ab}}{\mathrm{d}M^2 \mathrm{d}p_{\mathrm{T}}^2}(N) = \int_0^\infty \mathrm{d}b \frac{b}{2} W_{ab}(N+1, M^2, M^2\bar{b}^2, M^2/\mu^2), \quad (3.49)$$

with J_0 the first-order Bessel function. In this form, the $p_{\mathrm{T}} \to 0$ singularities are translated into large logarithms for $M\bar{b} \to \infty$ of the form

$$\left(\frac{1}{p_{\mathrm{T}}^2} \log^n \left(\frac{M^2}{p_{\mathrm{T}}^2} \right) \right)_+ \to \log^{m+1} M^2\bar{b}^2 + \dots \quad (3.50)$$

Following the CSS formalism [28], the Fourier-transformed cross section W_{ab} can be factorised as

$$W_{ab}(n, M^2, M^2\bar{b}^2, M^2/\mu^2) = \sum_{c,d} H_{cd}(M^2, M^2/\mu^2) S_{cd}(N, M^2\bar{b}^2) \times P_{c/a}(N, b^2, M^2\bar{b}^2) P_{d/b}(N, b^2, M^2\bar{b}^2) + \mathcal{O}\left(\frac{1}{M^2 b^2} \right), \quad (3.51)$$

where S_{cd} is an eikonal function that describes soft-gluon emission, $P_{c/a}$ is the parton-in-parton distribution at fixed transverse momentum, which includes the collinear singularities and will be later related to the p_{T}-integrated $\phi_{c/a}$ and H_{cd} is a hard function which is infrared-safe and can therefore be computed perturbatively,

$$H_{cd}(M^2, M^2/\mu^2) = \sum_{n=0}^{\infty} a_{\mathrm{S}}^n H_{cd}^{(n)}(M^2, M^2/\mu^2). \quad (3.52)$$

Although we have chosen a notation that highlights the similarities with threshold resummation, it is necessary to point out that the functions H_{cd} and S_{cd} are not defined as the ones in Eq. (3.23).

Solving the evolution equations for $P_{c/a}$ and the eikonal exponentiation, Eq. (3.51) gives

$$W_{ab}(N, M^2, M^2\bar{b}^2, M^2/\mu^2) = \sum_{c,d} H_{cd}(M^2, M^2/\mu^2) \times P_{c/a}(N, b^2, 1) P_{d/b}(N, b^2, 1) \exp(G_{cd}(M^2, M^2\bar{b}^2, M^2/\mu^2)), \quad (3.53)$$

where in this case the exponent G_{cd} can be written as

$$G_{cd}(M^2, M^2\bar{b}^2, M^2/\mu^2)$$
$$= -\frac{1}{2}\int_{1/\bar{b}^2}^{M^2}\frac{\mathrm{d}q^2}{q^2}\left(A_c(a_{\rm S}(q^2))\log\left(\frac{M^2}{q^2}\right) + B_c(a_{\rm S}(q^2))\right) + (c \leftrightarrow d), \quad (3.54)$$

and the $P_{c/a}$ functions can be expressed as

$$P_{c/a}(N^2, b, 1) = \sum_c C_{bc}(N, a_{\rm S}(1/\bar{b}^2)\phi_{c/a}(N, 1/\bar{b}^2). \quad (3.55)$$

Performing the inverse Fourier transform of W_{ab} and evolving the $\phi_{c/a}$ functions from the μ scale to $1/\bar{b}^2$ by using Eq. (3.15) we obtain

$$\sigma_{ab}(N, M^2, M^2/p_{\rm T}^2, M^2/\mu^2)$$
$$= \int_0^\infty \mathrm{d}b\frac{b}{2}J_0(bp_{\rm T})\sum_{c,d,e,f} H_{cd}(M^2, M^2/\mu^2)\exp(G_{cd}(M^2, M^2\bar{b}^2, M^2/\mu^2))$$
$$\times C_{ce}(N, a_{\rm S}(1/\bar{b}^2)C_{df}(N, a_{\rm S}(1/\bar{b}^2)E_{ea}(N, 1/\bar{b}^2, \mu^2)E_{fb}(N, 1/\bar{b}^2, \mu^2). \quad (3.56)$$

To perform the resummation at a given order, we need to perturbatively obtain the functions H_{ab}, A_a, B_a, C_{ab} at a given order in $a_{\rm S}$,

$$A_a = \sum_{n=1}^\infty a_{\rm S}^n A_a^{(n)}, \quad B_a = \sum_{n=1}^\infty a_{\rm S}^n B_a^{(n)}, \quad C_{ab}(N) = \delta_{ab} + \sum_{n=1}^\infty a_{\rm S}^n C_{ab}^{(n)}(N), \quad (3.57)$$

where for the LL accuracy we need the $H_{ab}^{(0)}, A_a^{(1)}$ terms, for the NLL the $H_{ab}^{(1)}, A_a^{(2)}, B_a^{(1)}, C_{ab}^{(1)}$ terms are also required, and for the NNLL also the terms $H_{ab}^{(2)}, A_a^{(3)}, B_a^{(2)}, C_{ab}^{(2)}$ are necessary. We will from now consider up to NLL corrections.

After the integration in Eq. (3.54) G_{ab} can be written as

$$G_{ab}(m^2, M^2\bar{b}^2, M^2/\mu^2) = \log(M^2\bar{b}^2 g_{ab}^{(1)}(\lambda)) + g_{ab}^{(2)}(\lambda, M^2/\mu^2) + \ldots, \quad (3.58)$$

with $\lambda := a_{\rm S}\beta_0\log(M^2\bar{b}^2)$. The function $g_{ab}^{(1)}$ resums up to LL and the $g_{ab}^{(2)}$ function resums the NLL contribution. These two functions are given by

$$2\lambda g_{ab}^{(1)}(\lambda) = (A_a^{(1)} + A_b^{(1)})(\lambda + \log(1-\lambda)), \quad (3.59)$$

$$\begin{aligned} 2\beta_0 g_{ab}^{(2)}(\lambda, M^2/\mu^2) = {} & (A_a^{(1)} + A_b^{(1)})\left(\frac{\lambda}{1-\lambda} + \log(1-\lambda)\right)\log\left(\frac{M^2}{\mu^2}\right) \\ & + (A_a^{(1)} + A_b^{(1)})\frac{\beta_1}{\beta_0}\left(\frac{\lambda + \log(1-1\lambda)}{1-\lambda} + \frac{1}{2}\log^2(1-\lambda)\right) \\ & - (A_a^{(2)} + A_b^{(2)})\frac{1}{\beta_0}\left(\frac{\lambda}{1-\lambda} + \log(1-\lambda)\right) \\ & + (B_a^{((1)} + B_b^{(1)})\log(1-\lambda), \end{aligned} \quad (3.60)$$

where the $A_a^{(i)}, B_a^{(i)}$ coefficients coincide with the values from threshold resummation in Eq. (3.38).

As a difference from threshold resummation, there is not a unique set of functions $H_{ab}^{(1)}, C_{ab}^{(1)}, B_a^{(2)}$ [29], but there is some freedom in the choice. We will use the original CSS factors [28, 30, 31], which are given by

$$H_{ab}(M^2, M^2/\mu^2) = \sigma_{ab}^{(0)}(M^2, M^2/\mu^2), \tag{3.61}$$

$$B_a^{(2)} = -2\delta P_{aa}^{(2)} + \beta_0 \left(\frac{2\pi^2}{3} C_a + \mathcal{A}_0 \right), \tag{3.62}$$

$$C_{ab}^{(1)}(N) = \delta_{ab} \left(C_a \frac{\pi^2}{6} + \frac{1}{2} \mathcal{A}_0 \right) - [P_{ab}^{(1)}(N)]_\epsilon, \tag{3.63}$$

where $[P_{ab}^{(1)}(N)]_\epsilon$ is the $\mathcal{O}(\epsilon)$ term in the ϵ-expansion of $P_{ab}^{(1)}$ and the other factors are defined as for threshold resummation.

Similarly to the case of threshold resummation, it is necessary to perform the matching, which in this case is given by

$$\hat{\sigma} = \hat{\sigma}_{\text{res}} + \hat{\sigma}_{\text{f.o.}} - \hat{\sigma}_{\text{exp}}, \tag{3.64}$$

with

$$\begin{aligned}
\hat{\sigma}_{ab}^{\text{exp}}(n, M^2, M^2/p_{\text{T}}^2, M^2/\mu^2) &= H_{ab}^{(0)}(M^2, M^2/\mu^2) + a_{\text{S}} H_{ab}^{(1)}(M^2, M^2/\mu^2) \\
-a_{\text{S}} \left(\mathcal{J} - \log \frac{M^2}{\mu^2} \right) \sum_c & (H_{ac}^{(0)}(M^2, M^2/\mu^2) P_{cb}^{(1)}(N) + P_{ca}^{(1)}(N) H_{cb}(M^2, M^2/\mu^2)) \\
&+ a_{\text{S}} \sum_c (H_{ac}^{(0)}(M^2, M^2/\mu^2) C_{cb}^{(1)}(N) + C_{ca}^{(1)}(N) H_{cb}^{(0)}(M^2, M^2/\mu^2)) \\
&- a_{\text{S}} H_{ab}^{(0)}(M^2, M^2/\mu^2) \left(\frac{\mathcal{J}^2}{4} (A_a^{(1)} + A_b^{(1)}) + \frac{\mathcal{J}}{2} (B_a^{(1)} + B_b^{(1)}) \right),
\end{aligned} \tag{3.65}$$

where

$$\mathcal{J} := \frac{1}{2} \int_0^\infty \mathrm{d}b \, J_0(b p_{\text{T}}) \log(M^2 \bar{b}^2). \tag{3.66}$$

Chapter 4

New gauge bosons

> *Ich gebe zu, dass mein Ausweg vielleicht von vornherein wenig wahrscheinlich erscheinen wird, weil man die Neutronen, wenn sie existieren, wohl schon längst gesehen hätte. Aber nur wer wagt, gewinnt.*[1]
>
> — Wolfgang Pauli in an open letter to the ETH Zürich proposing the existence of a new particle (the neutrino.)

The standard model (SM) of particle physics has proved extremely successful from a theoretical and experimental point of view. Its predictions have been confirmed up to a high precision and the recent landmark discovery of (a particle compatible with) the Higgs boson [1, 2] means the confirmation of the ideas of electroweak spontaneous symmetry breaking (SSB) and the theoretical closing of the SM. There are however numerous evidences that the SM is an incomplete theory. Examples of these include the hierarchy problem of the Higgs boson and the problem of dark matter, which cannot be explained in the context of the SM alone. Some of the most promising extensions which solve (some of these) problems of the SM involve additional gauge bosons similarly to the electroweak Z and W bosons.

In this chapter we will briefly introduce the most important theories and families of theories that include an additional Z' or additional Z' and W' bosons. There are many theories of this type, so this list by no mean complete, but we aim only to present those theories which are well established and that are interesting either from a theoretical or from a phenomenological point of view.

[1] *I admit that my solution may seem improbable because one would have probably seen those neutrons, should they exist, long time ago. But nothing ventured, nothing gained.* TN: What Pauli here calls the *neutron* would be later known as *neutrino.*

4.1 Theoretical models

Theories that include new heavy particles with spin-1 are only valid in quantum field theory (QFT) if the particle is a gauge boson associated with an spontaneous symmetry breaking [32]. The theory is defined by the specific breaking mechanism, which fixes the fermions charges under the new gauge symmetry, and (up to mixing terms) the couplings. Additional (exotic) fermions may be necessary in the theory for anomaly cancellations. We will study the phenomenology of various breaking schemes and the associated couplings to SM fermions.

The most general Lagrangian that can be written for Z' can be expressed as [32]

$$Z'_\mu(g_u^L\bar{u}_L\gamma^\mu u_L + g_d^L\bar{d}_L\gamma^\mu d_L + g_u^R\bar{u}_R\gamma^\mu u_R + g_d^R\bar{d}_R\gamma^\mu d_R + g_\nu^L\bar{\nu}_L\gamma^\mu\nu_L + g_e^L\bar{e}_L\gamma^\mu e_L + g_e^R\bar{e}_R\gamma^\mu e_R), \quad (4.1)$$

where u, d, ν, e are the SM fermions in the mass eigenstate basis and the g coefficients are real dimensionless parameters. In the case of generation-dependent couplings we would need to trivially introduce additional generation indices labelling the fermions and the coefficients would be promoted to 3×3 Hermitian matrices. For W' we have a similar expression [32],

$$\frac{W'^+_\mu}{\sqrt{2}}\left[\bar{u}_i(C^R_{q,ij}P_R + C^L_{q,ij}P_L)\gamma^\mu_j + \bar{\nu}_i(C^R_{l,ij}P_R + C^L_{l,ij}P_L)\gamma^\mu e_j)\right], \quad (4.2)$$

where the C coefficients are complex dimensionless parameters and for the SM quantities we use the same notation as in Eq. (4.1) and where we have now included the generation indices i, j explicitly.

4.1.1 The sequential standard model (SSM)

The most simple example of a theory including new gauge bosons Z' and W' is the sequential standard model (SSM) [33]. It is a non-realistic model that has the same couplings of the SM electroweak sector but with heavier gauge bosons. Despite being mainly non-physical, it is considered a standard for searchs in colliders and has been extensively used by experimental collaborations (see Ref. [34] and references therein).

For completeness and to fix notations we will write here the SSM couplings to SM fermions. In the case of the W' boson, the constants in Eq. (4.2) are simply given by

$$\begin{aligned} C^{\mathrm{L}}_{qij} &= g_{\mathrm{EW}}, \qquad C^{\mathrm{R}}_{qij} = 0, \\ C^{\mathrm{L}}_{lij} &= g_{\mathrm{EW}}, \qquad C^{\mathrm{R}}_{lij} = 0, \end{aligned} \quad (4.3)$$

where $i, j \in \{1, 2, 3\}$.

For Z' we can write the parameters in Eq. (4.1) as

$$\begin{aligned}
g_u^{\mathrm{L}} &= -\frac{g_{\mathrm{EW}}}{\cos\theta_{\mathrm{W}}}\left(\frac{1}{2}-\frac{2}{3}\sin^2\theta_{\mathrm{W}}\right), & g_u^{\mathrm{R}} &= -\frac{2g_{\mathrm{EW}}}{3\cos\theta_{\mathrm{W}}}\sin^2\theta_{\mathrm{W}},\\
g_d^{\mathrm{L}} &= -\frac{g_{\mathrm{EW}}}{\cos\theta_{\mathrm{W}}}\left(-\frac{1}{2}+\frac{1}{3}\sin^2\theta_{\mathrm{W}}\right), & g_d^{\mathrm{R}} &= \frac{g_{\mathrm{EW}}}{3\cos\theta_{\mathrm{W}}}\sin^2\theta_{\mathrm{W}},\\
g_e^{\mathrm{L}} &= -\frac{g_{\mathrm{EW}}}{\cos\theta_{\mathrm{W}}}\left(-\frac{1}{2}+\sin^2\theta_{\mathrm{W}}\right), & g_e^{\mathrm{R}} &= \frac{g_{\mathrm{EW}}}{\cos\theta_{\mathrm{W}}}\sin^2\theta_{\mathrm{W}},\\
g_\nu^{\mathrm{L}} &= -\frac{g_{\mathrm{EW}}}{2\cos\theta_{\mathrm{W}}}, & g_\nu^{\mathrm{R}} &= 0,
\end{aligned} \tag{4.4}$$

where θ_{W} is the Weinberg angle.

4.1.2 Grand Unification SU(5), SO(10) and E_6 models

The SM is based on the $\mathrm{SU(3)_c} \times \mathrm{SU(2)_L} \times \mathrm{U(1)}_Y$ symmetry group, which combines Quantum Chromodynamics (QCD) with the Glashow-Winberg-Salam theory of electroweak interactions. This symmetry group structure raises a number of theoretical concerns. On one hand it fails to unify the different forces and contains a relatively large number of arbitrary parameters. The fact that left-handed particles transform as doublets under $\mathrm{SU(2)_L}$ while right-handed ones transform as singlets, introduces an unnatural left-right asymmetry. Furthermore, the three-generation-structure lacks any theoretical explanation. Grand Unification Theories (GUT) attempt to solve (some of) these theoretical shortcomings.

Taking into account that the SM symmetry groups have rank 4, Georgi and Glashow [35] proposed SU(5) as the simples GUT. In $SU(5)$ the fermion fields are associated into $\bar{\mathbf{5}}$ and **10** representations. However, SU(5) was quickly ruled out experimentally by the proton lifetime and the electroweak mixing angle values [36].

SO(10) was proposed as the next-to-simplest GUT, which still remains compatible with experimental data. It embeds the SU(5) model and inherits some of its properties but includes additional right-handed neutrinos (see Ref. [37] and references therein).

Green and Schwarz showed that string theory is anomaly-free in ten dimensions if the gauge group is either $E_8 \times E_8'$ or SO(32). However, SO(32) does not lead to chiral fermions, so $E_8 \times E_8'$ seems more attractive from a phenomenological point of view. The compactification of the additional dimensions with SUSY $N = 1$ leads to E_6 as the effective symmetry group. Therefore, E_6 is now one of the most interesting GUT scenarios under study [37].

There exist a few E_6 breaking schemes, with different low-energy phe-

nomenology [38],

$$E_6 \to \mathrm{SO}(10) \times \mathrm{U}(1)_\psi \to \mathrm{SU}(5) \times \mathrm{U}(1)_\chi \times \mathrm{U}(1)_\psi, \tag{4.5a}$$
$$E_6 \to \mathrm{SU}(3)_c \times \mathrm{SU}(2)_\mathrm{L} \times \mathrm{U}(1)_Y \times \mathrm{U}(1)_\eta, \tag{4.5b}$$
$$E_6 \to \mathrm{SU}(3)_c \times \mathrm{SU}(2)_\mathrm{L} \times \mathrm{U}(1)_\mathrm{L} \times \mathrm{U}(1)_\mathrm{R}, \tag{4.5c}$$
$$E_6 \to \mathrm{SU}(3)_c \times \mathrm{SU}(2)_I \times \mathrm{U}(1)_Y \times \mathrm{U}(1)_{Y'}. \tag{4.5d}$$

We will focus in this section on model (4.5a) and in a later section (4.5c) will be reviewed in a general G(221) framework. For a general review, the reader is referred to Ref. [38] and references therein.

The E_6 and even a SO(10) symmetry would impose strong (often unrealistic) constraints and would lead to additional fermions for anomaly cancellations. We will not consider these issues here, but rather treat the models from a general and phenomenological point of view.

For model (4.5a), in general, a linear combination of Z_χ and Z_ψ will remain light,

$$Z' = Z_\chi \cos\beta + Z_\psi \sin\beta, \tag{4.6}$$

where β is a mixing parameter.[2]

The couplings to the SM fermions are given by [39]

$$\begin{aligned}
g_u^\mathrm{L} &= -g_\mathrm{EW}\frac{\cos\beta}{2\sqrt{10}} + g_\mathrm{EW}\frac{\sin\beta}{2\sqrt{6}}, & g_u^\mathrm{R} &= g_\mathrm{EW}\frac{\cos\beta}{2\sqrt{10}} - g_\mathrm{EW}\frac{\sin\beta}{2\sqrt{6}},\\
g_d^\mathrm{L} &= -g_\mathrm{EW}\frac{\cos\beta}{2\sqrt{10}} + g_\mathrm{EW}\frac{\sin\beta}{2\sqrt{6}}-, & g_d^\mathrm{R} &= -g_\mathrm{EW}\frac{3\cos\beta}{2\sqrt{10}} - g_\mathrm{EW}\frac{\sin\beta}{2\sqrt{6}},\\
g_\nu^\mathrm{L} &= g_\mathrm{EW}\frac{3\cos\beta}{\sqrt{40}} + g_\mathrm{EW}\frac{\sin\beta}{\sqrt{24}}, & g_\nu^\mathrm{R} &= 0,\\
g_e^\mathrm{L} &= g_\mathrm{EW}\frac{3\cos\beta}{2\sqrt{10}} + g_\mathrm{EW}\frac{\sin\beta}{2\sqrt{6}}, & g_e^\mathrm{R} &= g_\mathrm{EW}\frac{\cos\beta}{2\sqrt{10}} - g_\mathrm{EW}\frac{\sin\beta}{2\sqrt{6}}.
\end{aligned} \tag{4.7}$$

Some values of β give a Z' boson with special properties. Here we present some of the most important models included in this E_6 framework. For more details on specific models for different values of β, see Ref. [40].

1. The particular value $\beta = 0$, is called the Z_χ-model, and is the only family-universal model without additional particles (other than the right-handed neutrino) and without anomalies whose gauge group is orthogonal to $\mathrm{U}(1)_Y$.

2. In the case of $\beta = \pi/2$, the so-called Z_ψ-model, there are only axial vector couplings to SM fermions.

3. The case $\beta = -\arctan\sqrt{5/3}$, referred to in the literature as the Z_η-model, is the result of Calabi-Yau compatification of the heterotic string.

[2] Please note that in the literature the definition of β varies.

4. Another interesting case is $\beta = \arctan\sqrt{3/5}$, the so-called $-Z_I$-model, which has vanishing couplings to up-type quarks and is orthogonal to Z_η. In this model, the Z' production is suppressed at hadron colliders.

4.1.3 G(221) models

One of the families of models including both a Z' and a W' is obtained by extending the SM gauge groups with an additional SU(2). It can be viewed as a next-to-simplest extensions after the U(1) extensions seen in previous sections. Arguably the most studied model of this kind is the left-right model [41, 42, 43], but many other theoretical possibilities exist and they all yield very different low-energy phenomenology. It constitutes therefore an interesting goal of study at the LHC, and there are attempts to investigate the phenomenological consequences of these models from a global approach (see Ref. [44] and references therein).

Following the classification scheme of Hsieh et al. [44] we will generically review the G(221) models consisting of a gauge structure $\mathrm{SU}(2)_1 \times \mathrm{SU}(2)_2 \times \mathrm{U}(1)_X$ which breaks to the well-known electroweak SM sector $\mathrm{SU}(2)_L \times \mathrm{U}(1)_Y$ and eventually to $\mathrm{U}(1)_{\mathrm{em}}$ by spontaneous symmetry breaking (SSB). According to this classification we will consider two different breaking patterns:

1. In breaking pattern I, $\mathrm{SU}(2)_1$ is identified with the SM $\mathrm{SU}(2)_L$. Thus, the first breaking is $\mathrm{SU}(2)_2 \times \mathrm{U}(1)_X \rightarrow \mathrm{U}(1)_Y$, giving the W' and Z' bosons. The next breaking would be the usual SM SSB. To this set belong the left-right (LR), the leptophobic (LP), the hadrophobic (HP) and the fermiophobic (FP) models. The corresponding charges under the different simple groups are given in Tab. 4.1.

2. In breaking pattern II, $\mathrm{U}(1)_X$ is identified with $\mathrm{U}(1)_Y$ of the SM. Hence, the first breaking would be $\mathrm{SU}(2)_1 \times \mathrm{SU}(2)_2 \rightarrow \mathrm{SU}(2)_L$ giving the Z' and W' bosons, followed by the SM SSB. The charges under the different gauge groups are also summarized in Tab. 4.1. To this model belong the un-unified (UU) and non-universal (NU) models.

We will review now the theoretically distinguished LR models [41, 42, 43] and the left-handed UU [45] and NU models [46], to which we will restrict ourselves in the phenomenological study. We will explicitely not treat anomalies (which exist in the case of the UU model), but rather make a global analysis.

The left-right (LR) model

One of the best known theories predicting new gauge bosons involves restoring the left-right symmetry to the SM by introducing a new gauge group

Model	$SU(2)_1$	$SU(2)_2$	$U(1)_X$	
			quarks	leptons
Left-right	$(u_L, d_L), (\nu_L, e_L)$	$(u_R, d_R), (\nu_R, e_R)$	1/6	-1/2
Leptophobic	$(u_L, d_L), (\nu_L, e_L)$	(u_R, d_R)	1/6	Y_{SM}
Hadrophobic	$(u_L, d_L), (\nu_L, e_L)$	(ν_R, e_R)	Y_{SM}	-1/2
Fermiophobic	$(u_L, d_L), (\nu_L, e_L)$		Y_{SM}	Y_{SM}
Ununified	(u_L, d_L)	(ν_L, e_L)	Y_{SM}	Y_{SM}
Nonuniversal	$(u_L, d_L)_{1,2}, (\nu_L, e_L)_{1,2}$	$(u_L, d_L)_3, (\nu_L, e_L)_3$	Y_{SM}	Y_{SM}

Table 4.1: Charges of the different SM fermions under the G(221) symmetry groups for different models. From Ref. [44].

$SU(2)_R$. This models require a right-handed neutrino. In LR models left(right)-handed fermions transform as doublets under the additional $SU(2)_R$ group while right(left)-handed ones transform as singlets. There are many different specific realizations of this model (for a review see Ref. [47] and references therein), including manifest and pseudo-manifest LR, where the left-right symmetry is exact and therefore $g_L = g_R$, being the left CKM equal to the right CKM in the former case (but not the latter); and different models with no exact LR symmetry, where the LR symmetry is broken at a much higher scale.

Following Ref. [44] we will parametrize all the LR models by the introduction of three parameters $\{x, \phi, \beta\}$. The couplings cannot be directly expressed in terms of these parameters, so we will use the parameters $\{\phi, \theta, s_\phi := \sin\phi, g_X, g_1, g_2\}$ and later give the appropriate relations between the parameters. With this, the couplings of W' using the definitions in Eq. (4.2) are given by

$$\begin{aligned} C^L_{qij} &= g_2, \qquad C^R_{qij} = 0, \\ C^L_{lij} &= g_2, \qquad C^R_{lij} = 0, \end{aligned} \tag{4.8}$$

for $i, j \in \{1, 2, 3\}$. For Z' and using the definitions in Eq. (4.1), we have

$$\begin{aligned} g^L_u &= -\frac{1}{6} s_\phi g_X, & g^R_u &= \frac{1}{2} c_\phi g_2 - \frac{1}{6} s_\phi g_X, \\ g^L_d &= -\frac{1}{6} s_\phi g_X, & g^R_d &= -\frac{1}{2} c_\phi g_2 - \frac{1}{6} s_\phi g_X, \\ g^L_\nu &= \frac{1}{2} s_\phi g_X, & g^R_\nu &= \frac{1}{2} c_\phi g_2 + \frac{1}{2} s_\phi g_X, \\ g^L_e &= \frac{1}{2} s_\phi g_X, & g^R_e &= -\frac{1}{2} c_\phi g_2 + \frac{1}{2} s_\phi g_X, \end{aligned} \tag{4.9}$$

where $c_\phi := \cos\phi, s_\phi := \sin\phi$.

Now we can use the relations

$$\begin{aligned} \tan\phi &= \frac{g_2}{g_1}, \\ \sin^2(\theta)\cos^2(\theta) &= \frac{\pi\alpha_e}{\sqrt{2}M_z^2 G_F}, \\ \tan\theta &= g_X\left(\frac{1}{g_1^2}+\frac{1}{g_2^2}\right)^{1/2} \end{aligned} \tag{4.10}$$

to recover the dependence on the parameters $\{x, \phi, \beta\}$. For a complete derivation and constraints on the different parameters the reader is referred to Ref. [44].

An interesting example of LR model comes from a a particular breaking scheme for SO(10) (here embedded in E_6) as seen in Sec. 4.1.2. In this case the SO(10) group breaks into

$$\mathrm{SO}(10) \to \mathrm{SU}(3)_c \times \mathrm{SU}(2)_\mathrm{L} \times \mathrm{SU}(2)_\mathrm{R} \times \mathrm{U}(1)_{B-L}. \tag{4.11}$$

The couplings to the Z' in this case are given by just two parameters, since the other is fixed by the breaking scheme, and can be expressed as [39]

$$\begin{aligned} g_u^\mathrm{L} &= -\frac{1}{6\alpha}g_2, & g_u^\mathrm{R} &= \frac{\alpha}{2}g_2 - \frac{1}{6\alpha}g_2, \\ g_d^\mathrm{L} &= -\frac{1}{6\alpha}g_2, & g_d^\mathrm{R} &= -\frac{\alpha}{2}g_2 - \frac{1}{6\alpha}g_2, \\ g_\nu^\mathrm{L} &= \frac{1}{2\alpha}g_2, & g_\nu^\mathrm{R} &= 0, \\ g_e^\mathrm{L} &= \frac{1}{2\alpha}g_2, & g_e^\mathrm{R} &= -\frac{1}{2\alpha}g_2 - \frac{\alpha}{2}g_2, \end{aligned} \tag{4.12}$$

with α the free parameter

$$\alpha := \sqrt{\frac{\cos(\theta_\mathrm{W})}{\sin(\theta_\mathrm{W})}\frac{g_2^2}{g_1^2} - 1}, \tag{4.13}$$

where θ_W is the SM Weinberg angle. The parameter α lies in the range

$$\sqrt{\frac{2}{3}} \leq \alpha \leq \sqrt{\frac{\cos(\theta_\mathrm{W})}{\sin(\theta_\mathrm{W})} - 1}. \tag{4.14}$$

The ununified (UU) model

In the UU model the left-handed quarks and left-handed leptons are doublets under different SU(2) symmetry groups, being singlets for the other what gives raise to a mostly leptophobic left-handed W' boson, i.e., $C_{lij}^\mathrm{L} \ll C_{qij}^\mathrm{L}$ and $C_{lij}^\mathrm{R} = C_{qij}^\mathrm{R} = 0$.

The couplings in this model to the W' boson are given (with the same conventions as for the LR models) by [44]

$$\begin{aligned} C^{\mathrm{L}}_{qij} &= c_\phi g_1, \qquad C^{\mathrm{R}}_{qij} = 0, \\ C^{\mathrm{L}}_{lij} &= s_\phi g_2, \qquad C^{\mathrm{R}}_{lij} = 0, \end{aligned} \tag{4.15}$$

with $i, j \in \{1, 2, 3\}$.

For the Z' boson and using also the notations used for LR models, we obtain the following couplings [44]

$$\begin{aligned} g^{\mathrm{L}}_u &= \frac{1}{2} c_\phi g_1, \qquad g^{\mathrm{R}}_u = 0, \\ g^{\mathrm{L}}_d &= -\frac{1}{2} c_\phi g_1, \qquad g^{\mathrm{R}}_d = 0, \\ g^{\mathrm{L}}_\nu &= -\frac{1}{2} s_\phi g_2, \qquad g^{\mathrm{R}}_\nu = 0, \\ g^{\mathrm{L}}_e &= \frac{1}{2} s_\phi g_2, \qquad g^{\mathrm{R}}_e = 0. \end{aligned} \tag{4.16}$$

The UU models may have anomalies which need to be canceled by the introduction of exotic fermions. We will not enter into the details of such procedures since we are interested only in the couplings to SM fermions.

The non-universal (NU) model

Another left-handed model that predicts Z' and W' bosons is the NU, where the two light generation and the third one transform as doublets under different SU(2) groups and therefore the couplings are not generation-universal. For the parametrization of these models and the different constraints the reader is referred to Ref. [48].

We will, as with the other models, present here the couplings to the SM fermions. In the case of Z' the couplings, using the previous definitions can be expressed as [44]

$$\begin{aligned} g^{\mathrm{L}}_u &= \frac{1}{2} c_\phi g_1, \qquad g^{\mathrm{R}}_u = 0, \\ g^{\mathrm{L}}_d &= -\frac{1}{2} c_\phi g_1, \qquad g^{\mathrm{R}}_d = 0, \\ g^{\mathrm{L}}_\nu &= \frac{1}{2} c_\phi g_1, \qquad g^{\mathrm{R}}_\nu = 0, \\ g^{\mathrm{L}}_\nu &= -\frac{1}{2} c_\phi g_1, \qquad g^{\mathrm{R}}_e = 0. \end{aligned} \tag{4.17}$$

for the two light generations and

$$\begin{aligned} g_t^{\mathrm{L}} &= -\frac{1}{2}c_\phi g_2, & g_u^{\mathrm{R}} &= 0, \\ g_b^{\mathrm{L}} &= \frac{1}{2}s_\phi g_2, & g_d^{\mathrm{R}} &= 0, \\ g_\nu^{\mathrm{L}} &= -\frac{1}{2}s_\phi g_2, & g_\nu^{\mathrm{R}} &= 0, \\ g_\tau^{\mathrm{L}} &= \frac{1}{2}s_\phi g_2, & g_e^{\mathrm{R}} &= 0. \end{aligned} \tag{4.18}$$

for the third generation, while in the case of W' we have

$$\begin{aligned} C_{qij}^{\mathrm{L}} &= c_\phi g_1, & C_{qij}^{\mathrm{R}} &= 0, \\ C_{lij}^{\mathrm{L}} &= c_\phi g_1, & C_{lij}^{\mathrm{R}} &= 0, \end{aligned} \tag{4.19}$$

for the two light generations $i, j \in \{1, 2\}$ and

$$\begin{aligned} C_{q33}^{\mathrm{L}} &= s_\phi g_2, & C_{q33}^{\mathrm{R}} &= 0, \\ C_{l33}^{\mathrm{L}} &= s_\phi g_2, & C_{l33}^{\mathrm{R}} &= 0, \end{aligned} \tag{4.20}$$

for the third generation. As a difference with the UU model, these models do not present anomalies.

4.1.4 Other models

There are many other models than those here presented that predict new gauge bosons. One first example is the Little Higgs model [49] which predicts new particles, including not only new gauge bosons but fermions and Higgs bosons, which remove the one-loop divergencies to the SM Higgs mass solving the hierarchy problem. The details depend on the specific scenario. Another example of such theories would be the Kaluza-Klein excitations coming from extra dimensions. In technicolor theories, the techni-ρ is a non-elementary spin-1 boson which is a candidate for a composite Z'. A review of these different models can be found in the appropriate section of Ref. [32].

4.2 Current constraints

Experimental collaborations have searched for new gauge bosons in leptonic (e.g. LEP) as well as hadronic colliders, and it continues as one of the main focuses of exotic physics searches at the LHC. These searches give raise to several constraints on the Z' and W' bosons that we will briefly review.

4.2.1 Constraints on Z'

In leptonic colliders, Z' is produced in the process $e^+e^- \to f\bar{f}$ through an s-channel for $e \neq f$ and the s-, t-, and u-channel for $e = f$. In the case $M'_Z < \sqrt{s}$ it appears in the form of a resonance at the M'_Z mass (accompanied by a photon emission). The most important limits from this type of colliders come from LEP-II, and either set a lower limit $M'_Z > 209$ GeV or Z' couplings are of the order $\Gamma \sim \mathcal{O}(10^{-2})$ or lower. A review of the different limits can be found in Ref. [32] and references therein but are now largely outdated by LHC limits.

The most stringent limits on Z' currently come from LHC collaborations ATLAS and CMS. The Z' boson is expected to show up as a resonance in the dilepton channel that would determine the mass and width of the new boson. Furthermore, angular distributions by measurements of the rapidity would distinguish between couplings to up-type and down-type quarks, although the complete determination of the Z' couplings with 100 fb^{-1} of data at the design energy $\sqrt{s} = 14$ TeV is expected only for $m'_Z \leq 1.5$ TeV which is already ruled out for most of the important models as we will later see. The spin of the Z' boson could be measured under the same conditions for masses $m'_Z \leq 3 - 6$ TeV depending on the model [50, 51].

Two of the main channels are the e^+e^- and $\mu^+\mu^-$ which provide a good mass resolution. Current constraints coming from these channels combined are 2.33 TeV in the SSM, 2 TeV for the Z'_ψ E_6 model and similar values for other models by CMS at $\sqrt{s} = 7$ GeV [52]. Preliminar results from ATLAS at $\sqrt{s} = 8$ TeV claim limits of 2.49 TeV for the SSM, 2.09 TeV for Z'_ψ, 2.15 TeV for Z'_η and 2.24 TeV for Z'_χ E_6 models [53].

4.2.2 Constraints on W'

At leptonic colliders the W' boson must be produced in pairs via its Z and photon couplings. With LEP-II data the W' boson can be ruled out up to masses of 105 GeV [32].

Similarly to the Z' case, the main channel for W' searches is the leptonic decay to electron or muon and missing transverse energy. The mass of the W' boson can be seen as the endpoint of the transverse mass distribution. Usually the left-handed couplings are assumed to vanish, i.e., the $W - W'$ inteference is not considered, although the latest analyses by LHC have started to do so. Once discovered, however, the interference effects could be observed and would provide information about the couplings which could be used to determine the right model. The channel $\tau\overline{\nu}$ has not been explicitely investigated yet, although some information can be derived from missing transverse energy searches.

Other channels in which a W' boson can show up include the WZ, the $l^+l^- + jj$ channel in which the two jets and one lepton come from the decay

of a right-handed neutrino and the $t\bar{b}$ channel in the case of a heavy right-handed neutrino, i.e., when the decay of W' is kinematically forbidden my the right-handed neutrino mass.

Current constraints at LHC are at 2.5 TeV for a right-handed W' in the SSM by CMS at $\sqrt{s} = 7$ TeV and $2.43 - 2.64$ TeV when considering the interference with W in the leptonic channel [34], 840 GeV for a SSM W' in the $t\bar{t} + jj$ channel [54] also by CMS, and 2.55 TeV for SSM in the leptonic channel by ATLAS [55]. Preliminary results from CMS claim a 2.85 TeV limit in the leptonic channel for SSM with data at $\sqrt{s} = 8$ TeV [56].

Chapter 5

New gauge boson production at the LHC

In this chapter we will compute the fixed-order cross section for the the Drell-Yan-like leptonic channel.

We present the computation of the partonic cross section for new gauge boson production with leptonic decays (charged lepton-charged lepton for Z' and charged lepton-neutrino for W') at hadron colliders (i.e., with quarks and gluons in the initial state) up to next-to-leading order (NLO).[1]

5.1 Leading-order cross section

We will start by computing the leading-order contribution to $Z', \mathrm{W}'^{+}, \mathrm{W}'^{-}$ production, given, respectively, by the subprocesses

$$\begin{aligned} q\bar{q} &\to \gamma, Z, Z' \to l\bar{l}, \\ q\bar{q}' &\to W^{+}, \mathrm{W}'^{+} \to l^{+}\nu_l, \\ q\bar{q}' &\to W^{-}, \mathrm{W}'^{-} \to l^{-}\bar{\nu}_l. \end{aligned} \tag{5.1}$$

which are depicted generically in Fig. 5.1. The partonic cross section can be expressed as the corresponding squared matrix element averaged (summed) over all the incoming (outgoing) spins, polarizations and colous, multiplied by the final-state phase space and divided by the flux factor,

$$\mathrm{d}\sigma_{\mathrm{B}} = \frac{1}{36}\frac{1}{2s}|\overline{M_{\mathrm{B}}}|^2 \mathrm{dPS}^{(2)}. \tag{5.2}$$

Although it is not necessary at the LO level, we will perform the computations in $D = 4 - 2\epsilon$ dimensions for consistency with the NLO corrections.

[1] We will use the term next-to-leading order or NLO to refer to $\mathcal{O}(\alpha_{\mathrm{S}})$ corrections to the cross section. This definition varies in the literature, e.g., for transverse momentum (p_{T}) distributions.

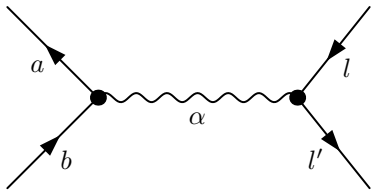

Figure 5.1: Feynman diagram 1 of the leading-order contribution to the Drell-Yan-like production of a vector boson $\alpha \in \{\gamma, Z, Z', W, \mathrm{W}'^{+}, \mathrm{W}'^{-}\}$ where l, l' are the appropriate (anti-)leptons and a, b represent the incoming (anti-)quark.

The differential phase space for two outoing particles with momenta p_1, p_2 can be written as

$$\mathrm{dPS}^{(2)} = \frac{1}{(2\pi)^{n-2}} \frac{\mathrm{d}^{D-1}k_1}{2E_1} \frac{\mathrm{d}^{D-1}k_2}{2E_2} \delta^n(p_1 + p_2 - k_1 - k_2). \tag{5.3}$$

If we substitute k_1, k_2 with the center-of-mass (COM) variables $y := (1 + \cos\theta)/2$ with θ being the angle formed by k_1, k_2 and $s = (p_1 + p_2)^2 = (k_1 + k_2)^2 =: Q^2$, we can integrate Eq. (5.3) taking into account that the Born matrix element will not depend on y.

To integrate Eq. (5.3) we will use the COM frame for k_1, k_2, with four-momentum

$$P_\mu^{\mathrm{COM}} = k_{1,\mu} + k_{2,\mu} = (\sqrt{s}, 0, 0, 0). \tag{5.4}$$

It can be seen that

$$\begin{aligned}
\int \mathrm{d}k_2 \delta(k_2^2 - m^2) &= \int \mathrm{d}k_2 \delta(E_2^2 - (|k_2|^2 + m^2) && (5.5)\\
&= \int \mathrm{d}k_2 \frac{1}{2\sqrt{|k_2|^2 + m^2}} \left(\delta\left(E_2 + \sqrt{|k_2|^2 + m^2}\right)\right. && (5.6)\\
&\quad \left. + \delta\left(E_2 - \sqrt{|k_2|^2 + m^2}\right)\right) && (5.7)\\
&= \frac{1}{2E_2}, && (5.8)
\end{aligned}$$

which can be inserted into Eq. (5.3) yielding

$$\begin{aligned}
\int \mathrm{dPS}^{(2)} &= \frac{\mathrm{d}^{D-1}k_1}{2E_1(2\pi)^{D-1}} \frac{\mathrm{d}^{D-1}k_2}{(2\pi)^{D-1}} (2\pi)^D && (5.9)\\
&\quad \times \delta((P - k_1)^2 - m^2) \delta^D(P - k_1 - k_2) && (5.10)\\
&= \frac{1}{(2\pi)^{D-2}} \int \frac{\mathrm{d}^{D-1}}{2E_1} \delta(s - E_1\sqrt{s} - m^2), && (5.11)
\end{aligned}$$

where we have used $k_2^2 = (P - p_1)^2 = s - 2E_1\sqrt{s}$. Now if we use polar coordinates in $D - 1$ dimensions,

$$\mathrm{d}^{D-1}k_1 = |k_1|^{D-2} \mathrm{d}|k_1| \mathrm{d}\Omega_{D-2} = E_1^{D-2} \mathrm{d}E_1 \mathrm{d}\Omega_{D-2} \tag{5.12}$$

and the identity [57]

$$\int \mathrm{d}\Omega_{D-1} \int \mathrm{d}\Omega_{D-2} \mathrm{d}\theta_{D-2} \sin^{D-2}\theta_{D-2} = \frac{2\pi^{(n-1)/2}}{\Gamma((n-1)/2)} \int \mathrm{d}\theta_{D-2} \sin^{D-2}\theta_{D-2}, \tag{5.13}$$

we obtain

$$\begin{aligned}\int \mathrm{dPS}^{(2)} &= \frac{1}{(2\pi)^{D-2}} \frac{1}{2} \int \mathrm{d}E_1 E_1^{D-3} \delta(s - 2E_1\sqrt{s} - m^2) \int \mathrm{d}\Omega_{D-2} \\ &= \frac{1}{(2\pi)^{D-2}} \frac{2\pi^{(D-2)/2}}{\Gamma((D-2)/2)} \frac{1}{2} \int \mathrm{d}E_1 E_1^{D-3} \int_0^\pi \mathrm{d}\theta \sin^{D-3}\theta \\ &\times \delta(s - s\sqrt{s}E_1 - m^2) \\ &= \frac{\pi^{(D-2)/2}}{(2\pi)^{D-2}\Gamma((n-2)/2)} \frac{1}{2\sqrt{s}} \left(\frac{s-m^2}{2\sqrt{s}}\right)^{D-3} \int \mathrm{d}\theta \sin^{D-3}\theta,\end{aligned} \tag{5.14}$$

where we have used

$$\delta(s - 2\sqrt{s}E_1 - m^2) \equiv \frac{1}{2s}\delta\left(E_1 - \frac{s-m^2}{2\sqrt{s}}\right). \tag{5.15}$$

Finally substituting $y := (1 + \cos\theta)/2$, we obtain

$$\int \mathrm{dPS}^{(2)} = \frac{1}{82} \frac{(4\pi)^\epsilon}{\Gamma(1-\epsilon)} \frac{(s-m^2)^{1-2\epsilon}}{s^{1-\epsilon}} \int_0^1 \mathrm{d}y [y(1-y)]^{-\epsilon}, \tag{5.16}$$

and since the Born matrix element does not depend on y, we can perform the integration,

$$\int_0^1 \mathrm{d}y [y(1-y)]^{-\epsilon} = \frac{\Gamma^2(1-\epsilon)}{(1-2\epsilon)\Gamma(1-2\epsilon)}, \tag{5.17}$$

so we finally obtain the relation

$$\int \mathrm{dPS}^{(2)} = \frac{1}{8\pi} \left(\frac{4\pi}{Q^2}\right)^\epsilon \frac{\Gamma(1-\epsilon)}{\Gamma(2-2\epsilon)}. \tag{5.18}$$

If we insert the identity

$$1 \equiv \int \mathrm{d}Q^2 \delta(s - Q^2) = \frac{1}{s} \int \mathrm{d}Q^2 \, \delta\left(1 - \frac{Q^2}{s}\right) \tag{5.19}$$

into Eq. (5.18) we obtain

$$\frac{\mathrm{dPS}^{(2)}}{\mathrm{d}Q^2} = \frac{1}{8\pi s} \left(\frac{4\pi}{Q^2}\right)^\epsilon \frac{\Gamma(1-\epsilon)}{\Gamma(2-2\epsilon)} \, \delta\left(1 - \frac{Q^2}{s}\right), \tag{5.20}$$

with what we can rewrite Eq. (5.2) as

$$\frac{\mathrm{d}\sigma_{\mathrm{B}}}{\mathrm{d}Q^2} = \frac{1}{36}\frac{1}{16s^2}|\overline{M_{\mathrm{B}}}|^2 \left(\frac{4\pi}{Q^2}\right)^{\epsilon} \frac{\Gamma(1-\epsilon)}{\Gamma(2-2\epsilon)}\,\delta\left(1-\frac{Q^2}{s}\right). \tag{5.21}$$

In the limit $\epsilon \to 0$ and using the definitions of Q^2 and y we recover the widely-known relation [13]

$$\frac{\mathrm{d}\sigma_{\mathrm{B}}}{\mathrm{d}t} = \frac{1}{36}\frac{1}{16s^2}|\overline{M_{\mathrm{B}}}|^2. \tag{5.22}$$

The squared matrix element is the sum of all the contributions of the different channels including all the possible interferences,

$$|\overline{M_{\mathrm{B}}}|^2 = \sum_a \sum_b \overline{M_a M_b^\dagger} \tag{5.23}$$

where $a, b \in \{\gamma, Z, Z'\}$ for the uncharged channel and $a, b \in \{W, W'\}$ for the charged channel.

The different terms can be read off the Feynman diagram in Fig. 5.1 using the usual Feynman rules,

$$\begin{aligned}\overline{M_a M_b^\dagger} = {} & \frac{1}{s - m_\alpha(m_\alpha + \Omega_\alpha)}\,\overline{\frac{1}{s - m_\beta(m_\beta - \Omega_\beta)}} \\ & \times \mathrm{Tr}[\gamma_\mu \Gamma_{\alpha qq} \not{p}_b \gamma_\nu \bar{\Gamma}_{\beta qq} \not{p}_a] \times \mathrm{Tr}[\gamma^\mu \Gamma_{\alpha ll} \not{p}_1 \gamma^\nu \bar{\Gamma}_{\beta ll} \not{p}_2],\end{aligned} \tag{5.24}$$

with α, β defined as before, m_α, Ω_α being the mass and width respectively of the vector boson α, $p_a(p_b)$ is the momentum of the incoming antiquark (quark), $p_1(p_2)$ is the momentum of the outgoing antilepton (lepton), $\Gamma_{\alpha qq}$ being the coupling of the vector boson α to two (anti-)quarks with the same or different colours and/or flavours and $\Gamma_{\alpha ll}$ being the coupling of the vector boson α to two charged (anti-)leptons with the same or different flavours. The different Γ couplings will have the general form

$$\Gamma := L\mathbb{P}_{\mathrm{L}} + R\mathbb{P}_{\mathrm{R}}, \tag{5.25}$$

with

$$\mathbb{P}_{\mathrm{L}} := \frac{1-\gamma_5}{2}, \quad \mathbb{P}_{\mathrm{R}} := \frac{1+\gamma_5}{2}, \tag{5.26}$$

and $\bar{\Gamma}$ is defined[2] to be

$$\bar{\Gamma} := L^*\mathbb{P}_{\mathrm{L}} + R^*\mathbb{P}_{\mathrm{R}}. \tag{5.27}$$

The different models have different Γ coupling factors. Introducing the Γ factors for a given model (which can be found in Ch. 4) into Eq. (5.24), substituting Eq. (5.23) into Eq. (5.2) and integrating over the appropriate range of Q^2 gives the final σ_{B}.

[2]Note that this is not the normal conjugate, which we will denote $\Gamma^\dagger$. We use this notation so the conjugate of a full vertex $\gamma_\mu\Gamma$ can be written as $(\gamma_\mu\Gamma)^\dagger = \Gamma^\dagger\gamma_\mu = \gamma_\mu\bar{\Gamma}$.

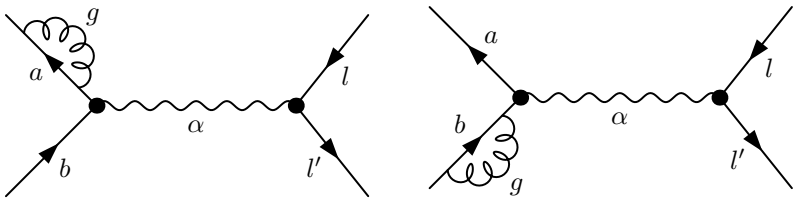

(a) Diagram 2.

(b) Diagram 3.

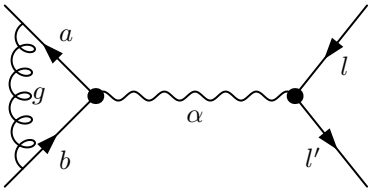

(c) Diagram 4.

Figure 5.2: Feynman diagrams of the next-to-leading order virtual contributions to the Drell-Yan-like production of a vector boson α. The notations are the same as in Fig. 5.1.

5.2 Next-to-leading order corrections

5.2.1 Virtual corrections

Virtual corrections at the NLO level come from virtual loops associated to the propagation of the incoming quarks (bubbles) and to the QCD vertex (triangle). The buble contributions will turn out to be zero.

The virtual cross section is given by a similar expression to Eq. (5.2)

$$\mathrm{d}\sigma_{\mathrm{v}} = \frac{1}{72s}|\overline{M_{\mathrm{v}}}|^2 \mathrm{dPS}^{(2)}. \tag{5.28}$$

so we can similarly write the differential cross section in D dimensions as

$$\frac{\mathrm{d}\sigma_{\mathrm{v}}}{\mathrm{d}Q^2} = \frac{1}{36}\frac{1}{16s^2}|\overline{M_{\mathrm{v}}}|^2 \left(\frac{4\pi}{Q^2}\right)^{\epsilon} \frac{\Gamma(1-\epsilon)}{\Gamma(2-2\epsilon)}\,\delta\left(1-\frac{Q^2}{s}\right). \tag{5.29}$$

Now we will compute the squared matrix elements for the different contributions.

For the bubble diagram the contribution will be zero. This can directly seen by considering the contribution to the incoming quark propagator, which will include a term of the form

$$\int \frac{\mathrm{d}^D k}{(2\pi)^D}\frac{1}{k^2(p-k)^2}, \tag{5.30}$$

which can only depend on p^2 since it must be a Lorentz scalar, and thus, in the massless quark limit,

$$\overline{M_2 M_1^{\dagger}} = 0. \tag{5.31}$$

Of course this can also be computed analytically obtaining the same result.

The triangle vertex in Fig. 5.2(c) can be expressed as

$$\Gamma^{\mu}_{\rm tr} = \int \frac{{\rm d}^D k}{(2\pi)^D} \frac{\gamma_\rho(\not{p}_a + \not{p}_b + \not{k})\gamma^\mu \not{k} \gamma^\rho}{((p_a+p_b+k)^2 k^2 (p_a+k)^2} \tag{5.32}$$

By using the defintions in Ref. [58] we can insert this into the interaction term of Fig. 5.2(c) with Fig. 5.1, obtaining

$$\begin{aligned}\overline{M_4 M_1^\dagger} = [4(p_a\cdot p_b)(C_{23}+C_{11}) + (2-D)^2 C_{24} \\ - 2(4-D)(p_a\cdot p_b)(C_{23}+C_{12})]\overline{M_1 M_1^\dagger}\end{aligned} \tag{5.33}$$

5.2.2 Real corrections

We will now investigate the NLO corrections arising from the emission of a real quark or gluon. In this case the final phase space has three particles, and therefore we have to use the expression

$${\rm d}\sigma_{\rm r} = \frac{1}{72s}|\overline{M_{\rm r}}|^2 {\rm dPS}^{(3)}, \tag{5.34}$$

where ${\rm dPS}^{(3)}$ represents the differential phase space for three particles, which can be expressed as

$${\rm dPS}^{(3)} = \frac{d^{D-1}k_1}{2E_1(2\pi)^{D-1}} \frac{d^{D-1}k_2}{2E_2(2\pi)^{D-1}} \frac{d^{D-1}k_3}{2E_3(2\pi)^{D-1}} (2\pi)^D \delta^D(p_1+p_2-k_1-k_2-k_3). \tag{5.35}$$

Using the expression [59]

$$1 = \int \frac{{\rm d}Q^2}{2\pi} \int \frac{d^{D-1}q}{(2\pi)^{D-1}2E_q} (2\pi)^D \delta^D(q-k_1-k_1), \tag{5.36}$$

where $q = k_1 + k_2$ represents an intermediate propagator, we can split the 3-particle phase space into two 2-particle phase spaces,

$$\begin{aligned}{\rm dPS}^{(3)} &= \frac{{\rm d}Q^2}{2\pi}\left[\frac{d^{D-1}k_3}{2E_3(2\pi)^{D-1}} \frac{d^{D-1}q}{2E_q(2\pi)^{D-1}} (2\pi)^D \delta^D(p_1+p_2-k_3-q)\right] \\ &\quad \times \left[\frac{d^{D-1}k_1}{2E_1(2\pi)^{D-1}} \frac{d^{D-1}k_1}{2E_1(2\pi)^{D-1}} (2\pi)^D \delta^D(q-k_1-k_2)\right] \\ &\equiv \frac{{\rm d}Q^2}{2\pi} {\rm dPS}^{(2)}_{\rm H} {\rm dPS}^{(2)}_{\rm L},\end{aligned} \tag{5.37}$$

where ${\rm dPS}^{(2)}$ has already been computed in Eq. (5.18) and using Eq. (5.16) we can write ${\rm dPS}^{(2)}_{\rm H}$ as

$${\rm dPS}^{(2)}_{\rm H} = \frac{1}{8\pi} \frac{(4\pi)^\epsilon}{\Gamma(1-\epsilon)} \frac{(s-Q^2)^{1-2\epsilon}}{s^{1-\epsilon}} \int_0^1 {\rm d}y \, (y(1-y))^{-\epsilon}, \tag{5.38}$$

where the y-integral cannot be performed yet since the squared matrix element for the virtual contributions will depend on y.

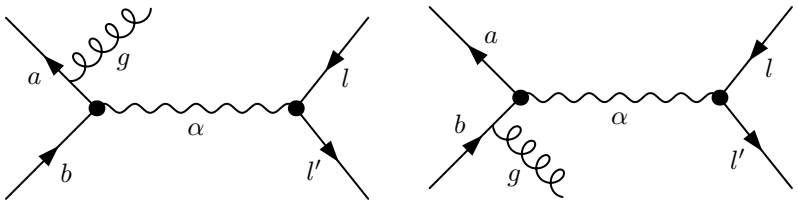

(a) Diagram 5. (b) Diagram 6.

Figure 5.3: Feynman diagrams of the NLO real gluon emission contributions to the Drell-Yan-like production of a vector boson α. The notations are the same as in Fig. 5.1.

Gluon emission

There are 2 different gluon emission diagrams contributing at the NLO level, as depicted in Fig. 5.3, which means there are 4 interference terms in the squared matrix element. We will compute here only one of the four elements (since the other three are very similar), and will include the full contribution in the final result.

Let us take the term associated to the squared matrix element given by the self-interference diagram in Fig. 5.3(a). From the Feynman diagram it can be read

$$\begin{aligned}\overline{M_5 M_5^\dagger} = &\left(\frac{1}{(p_a-k)^2-m_k^2}\right)^2 \frac{1}{s-m_\alpha(m_\alpha+\Omega_\alpha)}\frac{1}{s-m_\beta(m_\beta-\Omega_\beta)}\\ &\times \mathrm{Tr}[\gamma_\mu\Gamma_{\alpha qq}\not{p}_b\gamma_\nu\Gamma_{\beta qq}(\not{p}_a-\not{k})\gamma_\rho\not{p}_a\gamma^\rho(\not{p}_a-\not{k})]\\ &\times \mathrm{Tr}[\gamma^\mu\Gamma_{\alpha ll}(\not{p}_1-m_1)\gamma^\nu\Gamma_{\beta ll}(\not{p}_2+m_2)].\end{aligned} \tag{5.39}$$

Quark emission

In the case of quark emission there are 4 different diagrams contributing with a total of 8 inteference terms in the squared matrix elements. The different Feynman diagrams are depicted in Fig. 5.4.

As before, we will compute explicitely one of the terms, since the rest are very similar. Let us take the squared matrix element corresponding to the diagram in Fig. 5.4(a). From the Feynman diagram,

$$\begin{aligned}\overline{M_7 M_7^\dagger} = &\left(\frac{1}{s-m_q^2}\right)^2 \frac{1}{(p_a+p_b-k)^2-m_\alpha(m_\alpha+\Omega_\alpha)}\\ &\times \frac{1}{(p_a+p_b-k)^2-m_\beta(m_\beta-\Omega_\beta)}\\ &\times \mathrm{Tr}[\gamma_\mu\Gamma_{\alpha qq}(\not{p}_a+\not{p}_b)\gamma_\rho\not{p}_b\gamma^\rho(\not{p}_a+\not{p}_b)\gamma_\nu\Gamma_{\beta qq}\not{k}]\\ &\times \mathrm{Tr}[\gamma^\mu\Gamma_{\alpha ll}(\not{p}_1-m_1)\gamma^\nu\Gamma_{\beta ll}(\not{p}_2+m_2)].\end{aligned} \tag{5.40}$$

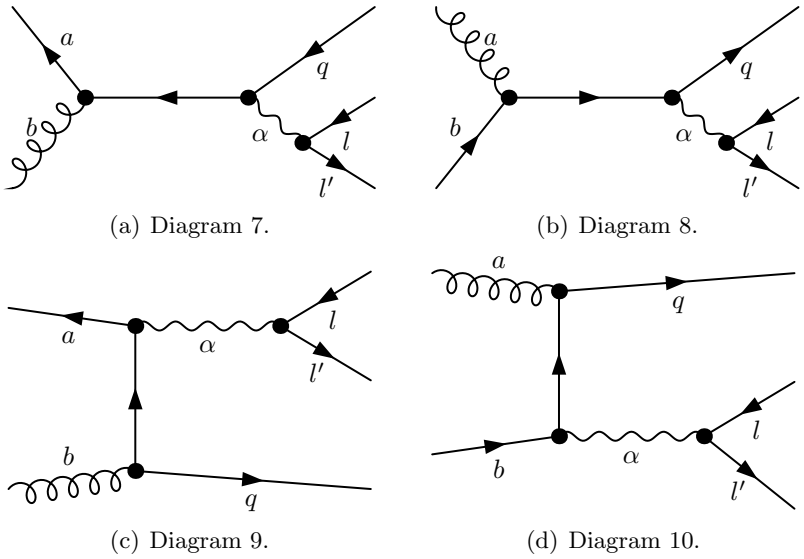

(a) Diagram 7. (b) Diagram 8.

(c) Diagram 9. (d) Diagram 10.

Figure 5.4: Feynman diagrams of the NLO real quark emission contributions to the Drell-Yan-like production of a vector boson α. The notations are the same as in Fig. 5.1, except that in this case a is a gluon in diagrams (c) and (d) and b is a gluon in diagrams (a) and (c).

The traces in every squared matrix element may been computed, e.g. by using software programs like `FORM` [60], but we will not included the full expression explicitely here.

Chapter 6

Numerical results

We will now present and analyze the numerical results obtained by implementing the results of Chs. 3 and 5 into a software program. For this we have modified and adapted a code originally developed by Debove [20] for gaugino production and the software has been used to obtain LO, NLO and resummation predictions for the production of Z' and W' with full interference in different models.

The implementation has been performed in a general way that let us easily compute predictions for the different models. For this work we have focused on prediction for the SSM because of its importance for experimental collaborations as well as the two left-handed models of the $G(221)$ family.

6.1 Sequential standard model

As stated before, the SSM provides a *standard candle* for experimental searches. Although not very well motivated from a theoretical point of view, its predictions are widely used by experimental collaborations to investigate and constrain new gauge boson properties and it is therefore a necessary benchmark model for universal analyses.

After analyzing LHC luminosities and current experimental constraints we have chosen two benchmark points for the SSM new gauge boson production. First, we will investigate the production of a Z' and W' bosons with SSM couplings to SM fermions and with masses $m'_Z = m'_W = 3$ TeV produced in a hadron collider with center-of-mass energy $\sqrt{S} = 8$ TeV. We will chose the factorization and renormalization scales to be $\mu_{\rm F}/m_{Z'} = \mu_{\rm R}/m_{Z'} = \mu/m_{Z'} = 1$ and use the scale variation $\mu/m_{Z'} \in [0.5, 2]$ to obtain the scale uncertainties. For the integrations we will choose a lower bound $Q_{\rm min} = \frac{3}{4} m_{Z'(W')}$ to separate our results from the SM background. As for the PDF we have chosen MSTW 2008 NLO [14] as it is considered a standard for LHC searches. We have used the values for the masses of the SM gauge bosons of $m_Z = 91.1876$ GeV and $m_W = 81.1876$ GeV and for the

Table 6.1: Total cross sections for new gauge boson production in a proton-proton collisions at a center-of-mass energy $\sqrt{S}$ at LO, NLO and resummation matched to NLO (NLO+NLL), using MSTW 2008 PDF. For the errors we have used scale variations $\mu_{\rm F}/m_{Z'} = \mu_{\rm R}/m_{Z'} = \mu/m_{Z'} \in \{0.5, 1, 2\}$ (first uncertainty) and the PDF errors obtained from Eqs. (6.1a) and (6.1b) (second uncertainty). The integration has a lower bound of $Q_{\rm min} = \frac{3}{4} m_{Z'(W')}$.

Boson	Mass	$\sqrt{S}$	$\sigma_{\rm LO}$ (ab)	$\sigma_{\rm NLO}$ (ab)	$\sigma_{\rm res}$ (ab)
Z'	3 TeV	8 TeV	$54.5^{+9.3}_{-7.5}$	$62.9^{+6.9+6.4}_{-6.0-2.6}$	$69.7^{+1.2+7.1}_{-0.6-2.8}$
W'^{+}	3 TeV	8 TeV	$310.1^{+55.4}_{-44.4}$	$275.7^{+31.3+40.0}_{-27.1-29.5}$	$310.7^{+1.8+43.2}_{-0.0-32.0}$
W'^{-}	3 TeV	8 TeV	$94.4^{+17.1}_{-13.7}$	$122.2^{+13.0+19.3}_{-11.5-11.4}$	$136.6^{+0.9+21.4}_{-0.2-12.4}$
Z'	4 TeV	14 TeV	$249.6^{+34.0}_{-28.4}$	$298.0^{+27.7+19.8}_{-23.9-7.7}$	$321.5^{+10.2+19.8}_{-9.3-9.4}$
W'^{+}	4 TeV	14 TeV	$1274.3^{+182.0}_{-149.7}$	$1406.7^{+129.1+68.7}_{-110.2-44.0}$	$1367.0^{+130.3+256.2}_{-0.0-42.0}$
W'^{-}	4 TeV	14 TeV	$375.3^{+52.6}_{-44.3}$	$489.4^{+45.9+48.3}_{-37.3-19.6}$	$523.1^{+14.5+114.7}_{-5.8-21.1}$

top quark mass $m_q = 171.1$ GeV [32] and vanishing masses for the five light quarks. The errors for the PDF variation are obtained using the expressions defined by the MSTW collaboration [14],

$$\Delta^2\sigma_{\rm up} = \sum_{k=1}^{n} \left(\max(\sigma_k^+ - \sigma_0, \sigma_k^- - \sigma_0, 0)\right)^2, \tag{6.1a}$$

$$\Delta^2\sigma_{\rm down} = \sum_{k=1}^{n} \left(\max(\sigma_0 - \sigma_k^+, \sigma_0 - \sigma_k^-, 0)\right)^2, \tag{6.1b}$$

with σ_0 being the value of the cross section using the central set of the PDF, and $\sigma_k^{\pm}$ are the values obtained from the $\pm\sigma$ variation along the k-eigenvector of the covariance matrix of the PDF fit.

The total cross sections for the first benchmark point are presented in Tab. 6.1. We show the LO, NLO and threshold resummation matched to NLO (NLO+NLL) computations for the production of Z' and $W'^{\pm}$. The cross sections include the contribution of all the SM channels, i.e., include the contribution from γ, Z channels in the case of Z' and the W boson in the case of the W' production. We can see that in the case of Z' production resummation corrections mean a 10% value with respecto to fixed-order NLO predictions, and almost 30% with respect to LO computations. Resummation corrections are also of the order $\sim 10\%$ in the case of $W'^{\pm}$ production with respect to NLO predictions. We can see that final resummed cross section is ~ 4.5 times bigger in the case of W' than in the case of Z', which justifies the necessity for high-precision W' predictions. Even the cross section for W'^{-}, which is lower than the W'^{-} cross section by a factor ~ 2.3 (we are dealing with a proton-proton collision), is greater than for Z'.

Apart from the predictions given for the current center-of-mass energy of $\sqrt{S} = 8$ TeV we have also computed predictions for a second benchmark

point at the designed energy of the LHC of $\sqrt{S} = 8$ TeV. In this case we have chosen a boson mass of 4 TeV based on projected luminosities. The rest of the parameters are the same as in the first benchmark point. The numerical results for the cross sections are also presented in Tab. 6.1. We can see that the effects on resummation on the cross section with respect to NLO computations are of the order $3 - 7\%$ in this case, which is to be expected, since in this case the relation of the energies with respect to boson mass is bigger and therefore we are farther from the threshold, where resummation contributions are important.

Apart from total cross sections, there are other important predictions used by experimental collaborations to discover and determine the properties of a new particle. Important examples are the transverse momentum (p_{T}) and invariant mass (M) distributions. In this work we will focus of transverse momentum distributions $\mathrm{d}\sigma/\mathrm{d}p_{\mathrm{T}}$ for their experimental relevance and the role of transverse momentum resummation formalism.

Fixed-order (in this case NLO) contributions are divergent in the limit $p_{\mathrm{T}} \to 0$ and unreliable in the low-p_{T} kinematical region because of large logarithmic factors that spoil the convergence of the series. These terms can be resummed using the formalism presented in Sec. 3.3, therefore restoring the convergence properties of the series and giving reliable results. An example of this can be seen in Fig. 6.1(a), where we have plotted the NLO and transverse momentum resummation matched to NLO (NLO+NLL) predictions for the production of a Z' in the first benchmark point at (relatively) low transverse momentum (p_{T}). Please note that at LO, $p_{\mathrm{T}} = 0$, since there is no emitted gluon or quark that could carry transverse momentum, and therefore the produced lepton-pair cannot acquire transverse momentum either. We have included the error bands for scale variation and from PDF uncertainties as previously defined. We can see that at low-p_{T} the NLO contribution diverges while at NLO+NLL a finite peak is predicted. Similar results are also shown for $W'^{\pm}$ production also in the first benchmark point in Fig. 6.2 and for the second benchmark point in Fig. 6.3. In Fig. 6.4 we have plotted the transverse momentum distributions for W'^{+} together with the results for W'^{-} to show the asymmetry due to the proton-proton collion.

We will now analyse the uncertainties due to scale variation and PDF fit. In Fig. 6.5(a) we have plotted the mean scale and PDF uncertainties, defined as

$$\varepsilon := \frac{1}{2}\frac{\Delta^{\mathrm{up}} + \Delta^{\mathrm{down}}}{\mathrm{d}\sigma/\mathrm{d}p_{\mathrm{T}}} \tag{6.2}$$

for the transverse momentum distribution in the production of a W'^{+} at NLO and NLO+NLL with the parameters for the second benchmark point as previously defined. We can see that the PDF error is constant at about $\sim 5\%$ in the case of NLO and vanishing in the $p_{\mathrm{T}} \to 0$ limit and increasing up to $\sim 10\%$ for $p_{\mathrm{T}} = 150$ GeV in the NLO+NLL case. The fact that it

vanishes at low p_{T} is due to the fact that transverse momentum resummation resums all the logarithmic terms in that limit, and the fact that the uncertainty is larger than in the NLO case for higher values of transverse momentum is due to the fact that resummation, due the Mellin transform applied to the parton distribution functions, probes a larger region of the x-space, and in particular regions where the uncertainties are larger due to experimental constraints. The scale uncertainty, which depends only on theoretical considerations remains constant at $\sim 20\%$ in the NLO case, and has a maximum at $\sim 6-7\%$ at around $p_{\mathrm{T}} \sim 60$ GeV in the case of NLO+NLL, remaining stable at larger values and vanishing in the low p_{T} limit.

The reason for the lower uncertainty in the NLO+NLL case can be seen from the dependence of the final cross section on the unphysical and arbitrary scales. We assume the simplifcation $\mu_{\mathrm{F}} = \mu_{\mathrm{R}} = \mu$ and plot the cross section with respect to μ in Fig. 6.5(b) for Z' production as defined in the second benchmark point. It can be clearly seen that the cross section heavily depends on the scale in the LO case, meaning that results are not realiable (or that the uncertainties are large) in that case. In the case of NLO, the scale dependence is also manifest, while the dependece is much more under control in the NLO+NLL case, leading to the lower uncertainties as previously seen.

Finally we show in Fig. 6.6(a) the total cross section for the production of a Z' under the same conditions of the second benchmark point, except that the mass of the new gauge boson m'_Z varies in the range $1-5$ GeV and the lower bound for the integration varies accordingly. Please note that some of these masses are already excluded by LHC data (see Sec. 4.2.1). As expected the cross section decays for large boson mass because of the boson propagator and because of the limits of intergration. More interestingly, as the boson mass increases, the difference between the center-of-mass energy and the threshold is reduced, and thus the resummation effects become more important, as can be seen in Fig. 6.6(b).

In the rest of the chapter we will present the results for the left-handed G(221) models presented in Sec. 4.1.3.

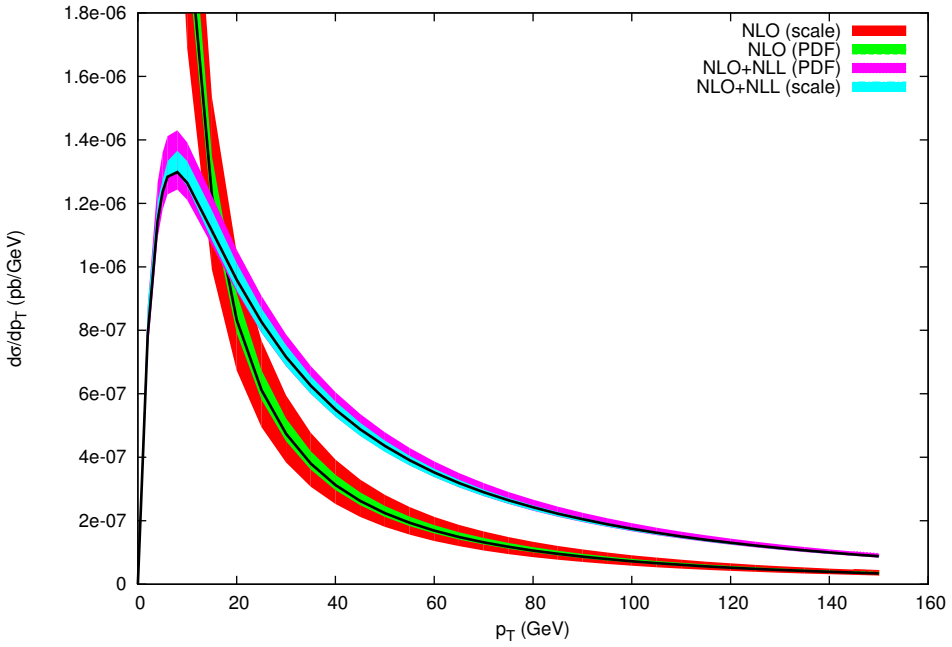

(a)

Figure 6.1: Transverse momentum distribution for the production of a Z' boson with a mass of 3 TeV in a proton-proton collision at a center-of-mass energy (a) $\sqrt{S} = 8$ TeV in the sequential standard model using the MSTW2008NLO PDF at the next-to-leading order and next-to-leading order matched with resummation, including error bands for PDF uncertainties and scale variations for $\mu_{\mathrm{F}}/m_{Z'} = \mu_{\mathrm{R}}/m_{Z'} = \mu/m_{Z'} \in \{0.5, 1, 2\}$.

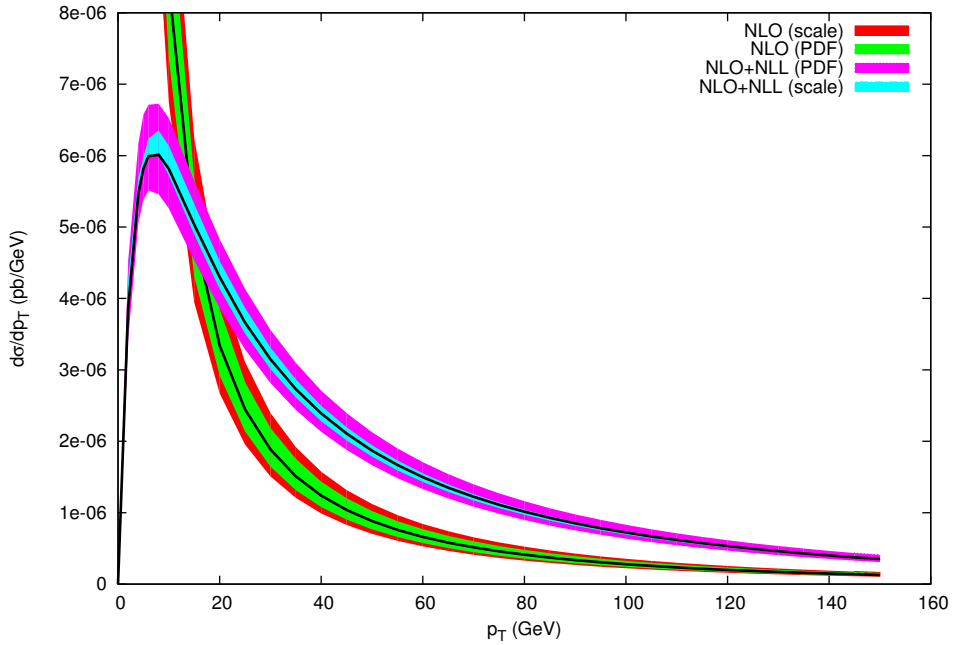

(a)

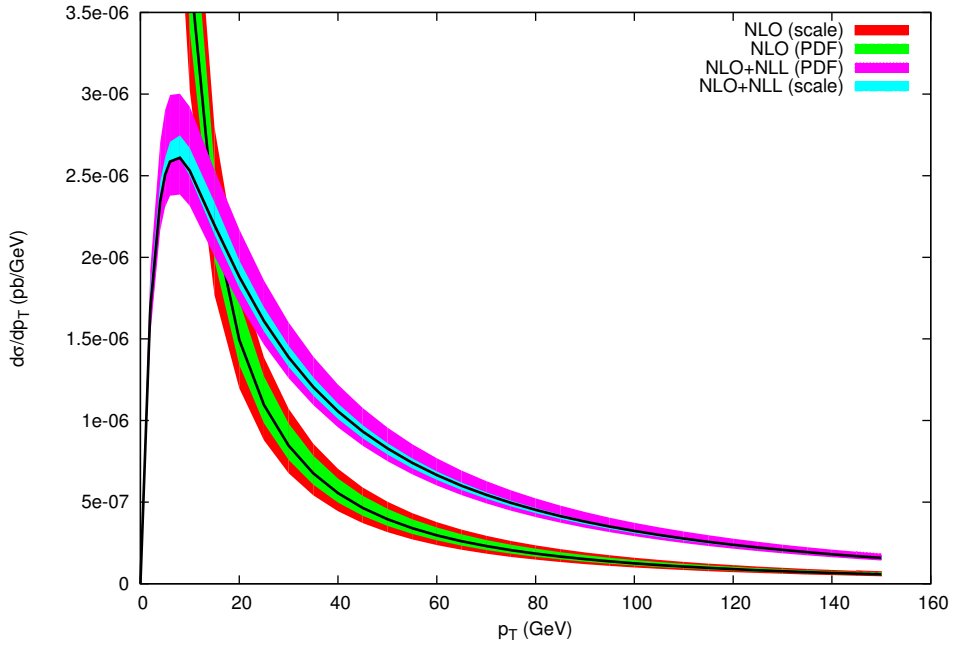

(b)

Figure 6.2: Transverse momentum distribution for the production of (a) W'^{+} and (b) W'^{-} boson with a mass of 3 TeV at a center-of-mass-energy of 8 TeV. The rest of parameters and error bands are the same as in Fig. 6.1.

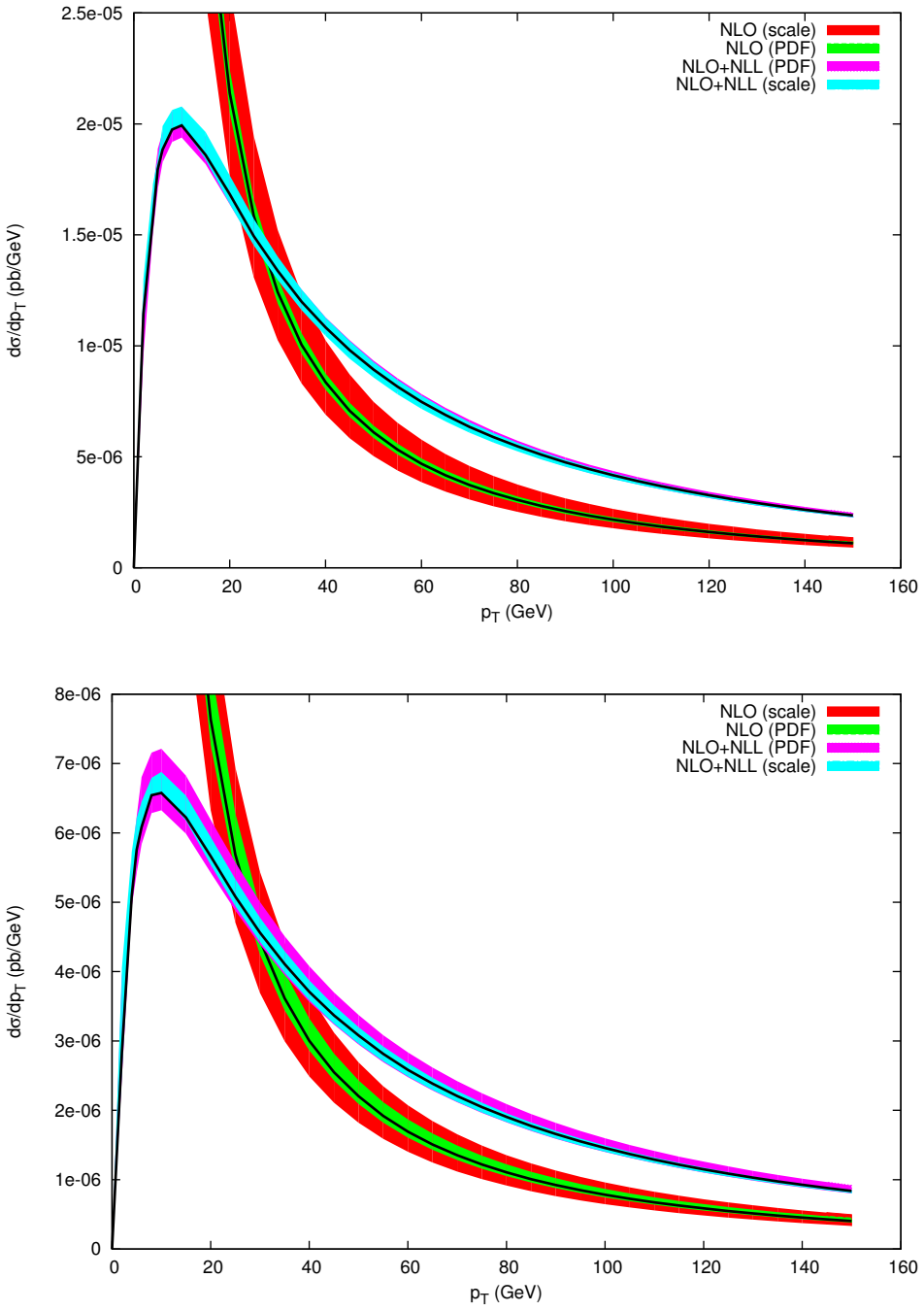

Figure 6.3: Transverse momentum distribution for the production of (a) W'^{+} and (b) W'^{-} boson with a mass of 4 TeV at a center-of-mass-energy of 14 TeV. The rest of parameters and error bands are the same as in Fig. 6.1.

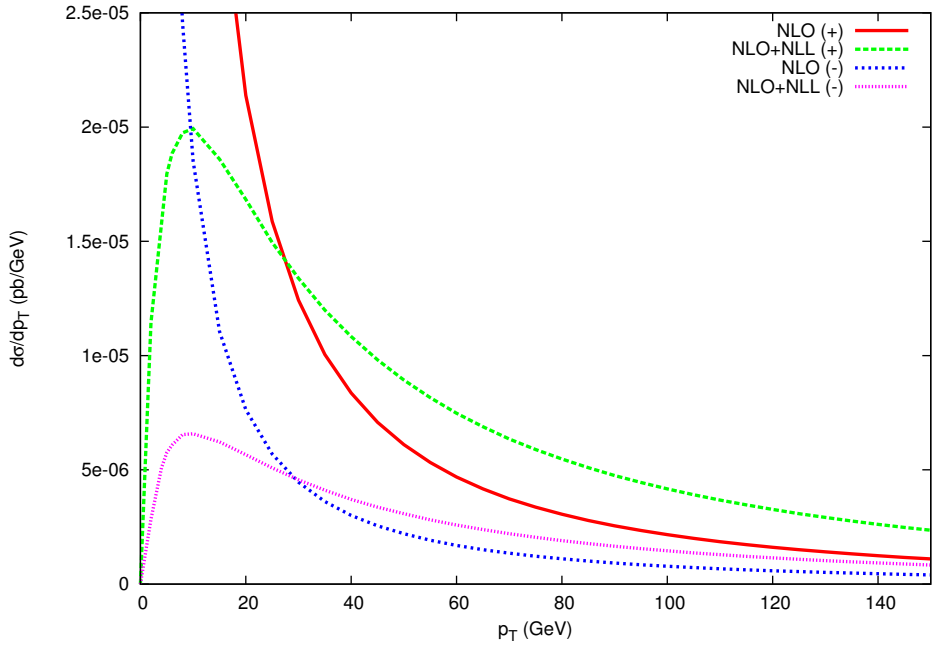

(a)

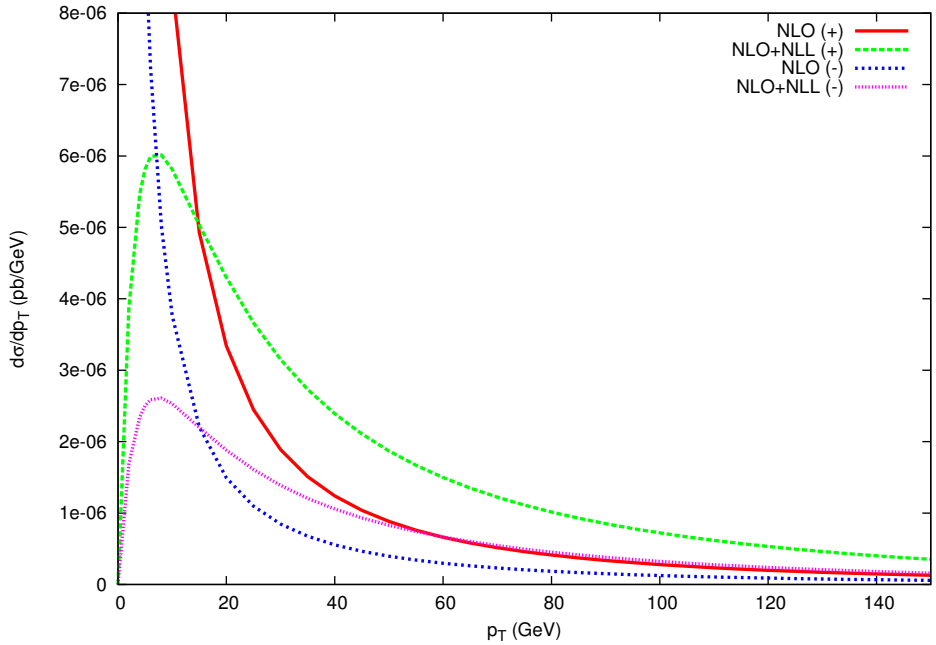

(b)

Figure 6.4: Comparison of transverse momentum distributions for W'^{+} and W'^{-} with a mass of (a) 3 TeV and (b) 4 TeV at a center-of-mass energy of (a) 8 TeV and (b) 14 TeV. The rest of parameters are the same parameters as in Fig. 6.1.

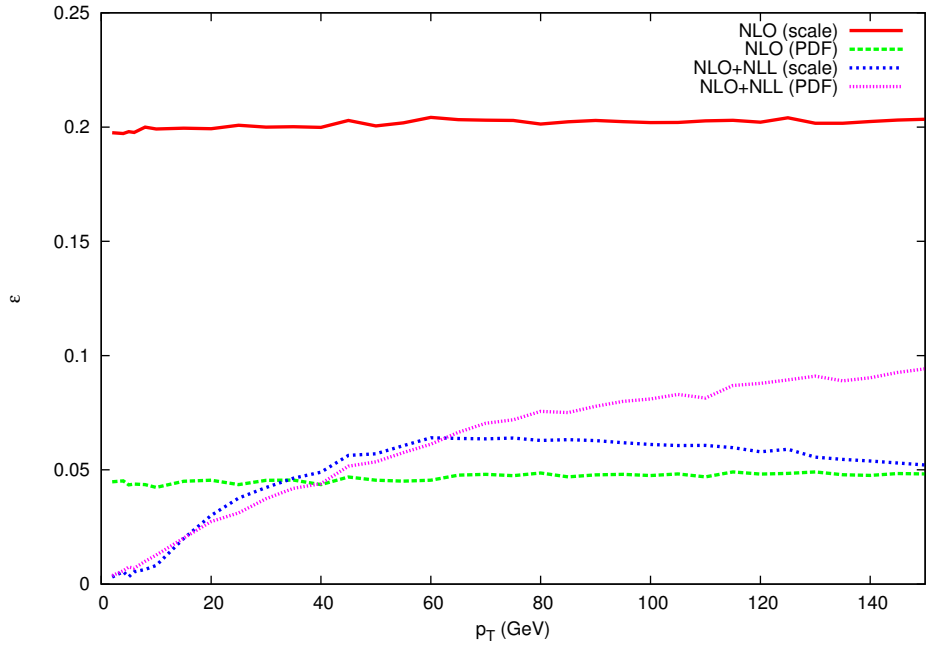

(a)

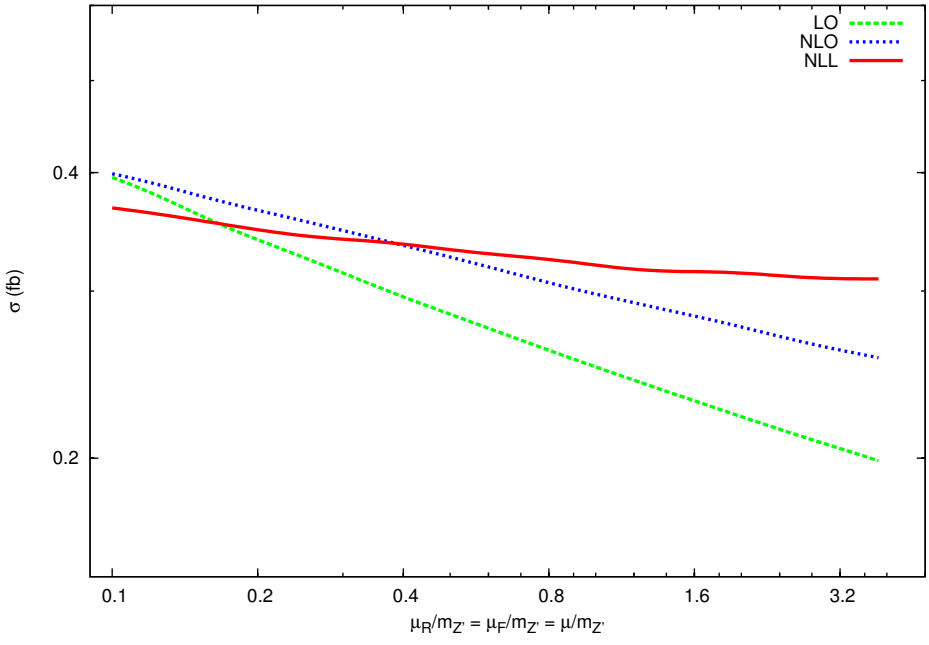

(b)

Figure 6.5: (a) Mean relative uncertainty $\varepsilon := \frac{1}{2}\frac{\Delta^{\mathrm{up}}+\Delta^{\mathrm{down}}}{\mathrm{d}\sigma/\mathrm{d}p_{\mathrm{T}}}$ of the transverse momentum distribution for W'^{+} production with a mass of 4 TeV at a center of mass energy $\sqrt{S} = 14$ TeV with the same parameters as in Fig 6.1 and (b) variation of the total cross section for the production of a 4 TeV Z' in a proton-proton collision at center-of-mass energy 14 TeV with respect to the scale $\mu_{\mathrm{F}}/m_{Z'} = \mu_{\mathrm{R}}/m_{Z'} = \mu/m_{Z'}$. The rest of parameters are the same as in Fig. 6.1.

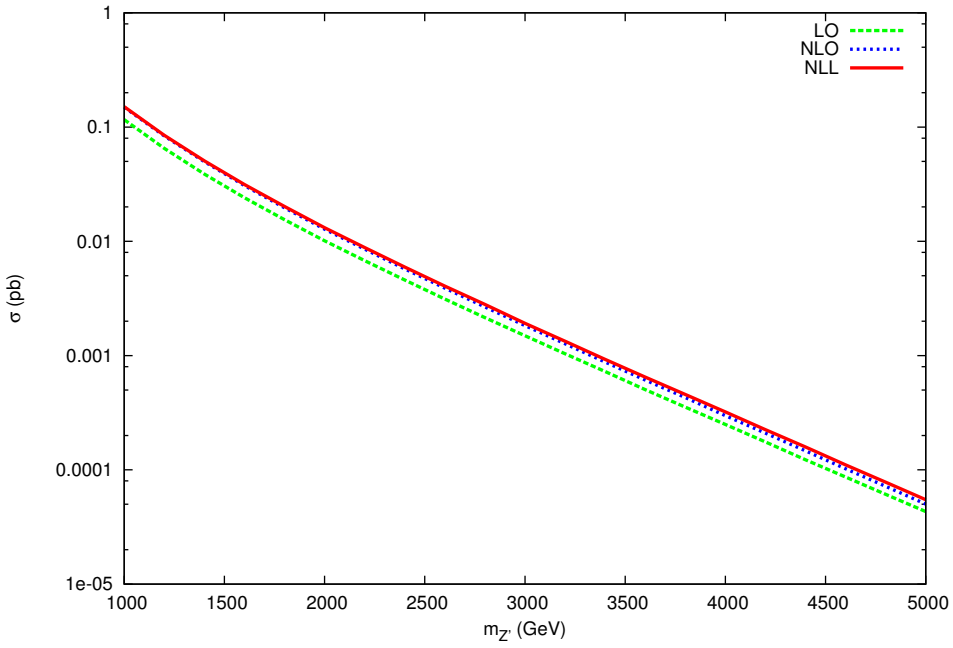

(a)

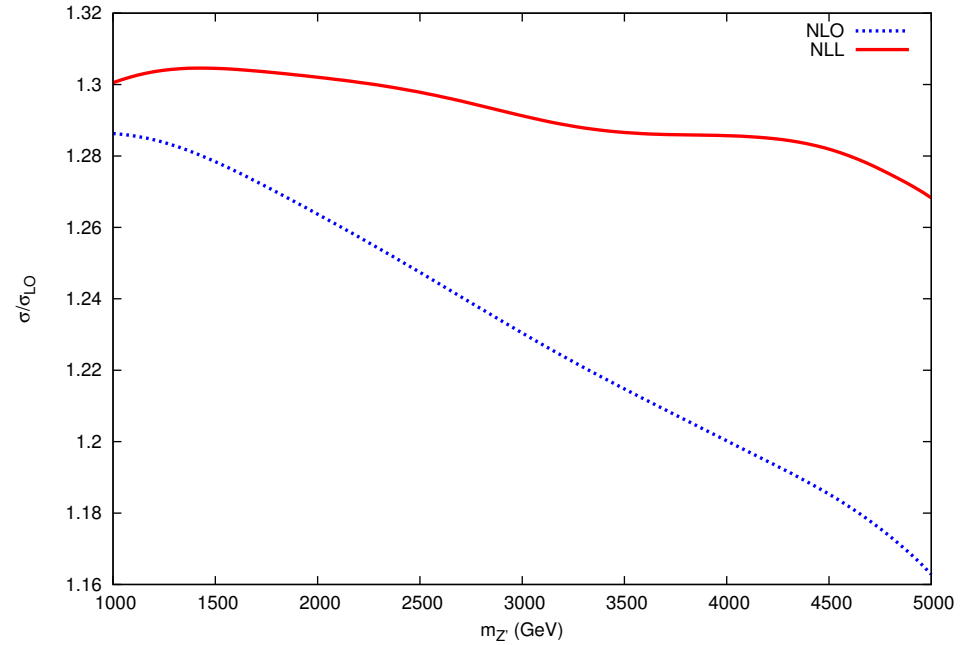

(b)

Figure 6.6: (a) Total cross section and (b) ratio of the cross section and the LO cross section for the production of a 4 TeV Z' in a proton-proton collision at center-of-mass energy 14 TeV with respect to the boson mass $m_{z'}$. The rest of parameters are the same as in Fig. 6.1.

6.2 The ununified model

We will now discuss the results obtained for the ununified model. For this model we have chosen for practical purposes the reparametrisation done in Ref. [48], in which models are defined by the new gauge boson mass $m_{Z'(W')}$ and a free parameter t. This parameter t is constrained by the analysis done in Ref. [44] and according to these contraints we have chosen six benchmark points. First, for the current center-of-mass energy $\sqrt{S} = 8$ TeV and with a new gauge boson of mass $m_{W'} = 3$ TeV we have chosen three values of t in the allowed parameter space, namely $t \in \{0.2, 0.4, 0.6\}$. And for the design center-of-mass energy of $\sqrt{S} = 14$ TeV and a new gauge boson mass of 4 TeV we have chosen three t values in the allowed parameter space, $t \in \{0.4, 0.7, 1.2\}$. These t values have been chosen to achieve as much overlap as possible between the different energies and with the following nonunified model, while covering as much of the interesting parameter space as possible. For these models we have focused on W' production, since it would be found earlier at the LHC, but a similar analysis also holds for Z' production.

The summary of the benchmark points and the corresponding total cross sections can be found in Tab. 6.2. The cross sections have been computed using the same parameters and the same analysis for uncertainties as with the SSM. We also show the transverse-momentum distributions of the $W'^{\pm}$ for the six benchmark points chosen in Figs. 6.7 and 6.8. In this case only scale uncertainties are shown for simplification.

Table 6.2: Benchmark points and the corresponding total cross sections for $W'^{\pm}$ in the ununified model. The parameters and uncertainties are defined as in Tab. 6.1.

Boson	Mass	$\sqrt{S}$	t	σ_{LO} (ab)	σ_{NLO} (ab)	σ_{res} (ab)
W'^{+}	3 TeV	8 TeV	0.2	$32.5^{+5.1}_{-4.2}$	$24.8^{+4.4+1.8}_{-3.5-1.4}$	$29.0^{+1.4+1.9}_{-0.7-1.5}$
W'^{-}	3 TeV	8 TeV	0.2	$9.7^{+1.5}_{-1.2}$	$9.4^{+1.6+1.2}_{-1.3-0.6}$	$10.8^{+0.6+1.3}_{-0.3-0.6}$
W'^{+}	3 TeV	8 TeV	0.4	$124.1^{+20.3}_{-16.5}$	$103.6^{+15.6+9.1}_{-12.7-7.1}$	$119.1^{+4.0+9.8}_{-2.0-7.6}$
W'^{-}	3 TeV	8 TeV	0.4	$37.3^{+6.1}_{-4.9}$	$41.0^{+5.9+5.4}_{-4.9-2.9}$	$46.5^{+1.8+6.1}_{-1.0-3.1}$
W'^{+}	3 TeV	8 TeV	0.6	$224.2^{+37.9}_{-30.5}$	$193.7^{+26.1+20.4}_{-21.9-15.9}$	$221.0^{+5.0+21.9}_{-2.3-17.1}$
W'^{-}	3 TeV	8 TeV	0.6	$67.7^{+11.5}_{-9.3}$	$79.7^{+10.3+11.2}_{-8.8-6.3}$	$89.8^{+2.4+12.5}_{-1.3-6.8}$
W'^{+}	4 TeV	14 TeV	0.4	$387.2^{+50.9}_{-42.5}$	$386.7^{+47.2+15.2}_{-39.5-8.3}$	$397.9^{+18.0+51.3}_{-0.0-9.2}$
W'^{-}	4 TeV	14 TeV	0.4	$114.7^{+14.9}_{-12.5}$	$130.4^{+15.5+11.1}_{-13.0-4.6}$	$139.2^{+7.0+21.6}_{-3.1-4.7}$
W'^{+}	4 TeV	14 TeV	0.7	$974.8^{+133.4}_{-110.9}$	$1037.8^{+108.0+44.6}_{-93.7-26.8}$	$1041.3^{+56.3+166.0}_{-0.0-28.9}$
W'^{-}	4 TeV	14 TeV	0.7	$288.0^{+39.0}_{-32.5}$	$355.1^{+36.0+32.7}_{-31.2-13.5}$	$377.3^{+13.5+69.5}_{-4.9-13.7}$
W'^{+}	4 TeV	14 TeV	1.2	$1722.2^{+240.2}_{-199.2}$	$1866.7^{+188.2+87.5}_{-154.1-50.0}$	$1851.4^{+133.5+324.2}_{-0.0-56.1}$
W'^{-}	4 TeV	14 TeV	1.2	$510.9^{+69.5}_{-59.2}$	$642.4^{+64.5+61.1}_{-51.2-22.2}$	$681.6^{+23.9+135.1}_{-3.8-22.6}$

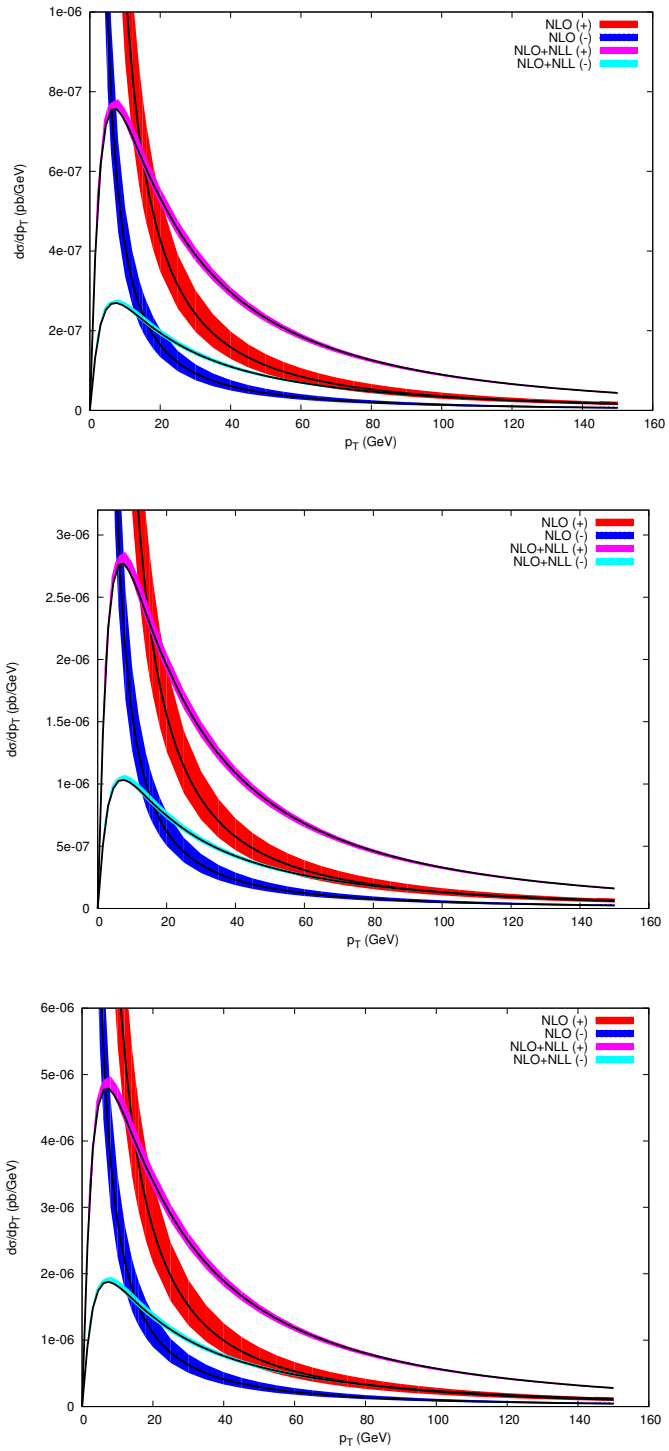

Figure 6.7: Transverse-momentum distribution for the production of $W'^{\pm}$ bosons of mass 3 TeV in a proton-proton collider at a center-of-mass-energy of 8 TeV in the UU model for parameter t of (from top to bottom) 0.2, 0.4 and 0.6. The rest of the parameters are the same as in Fig. 6.1.

.

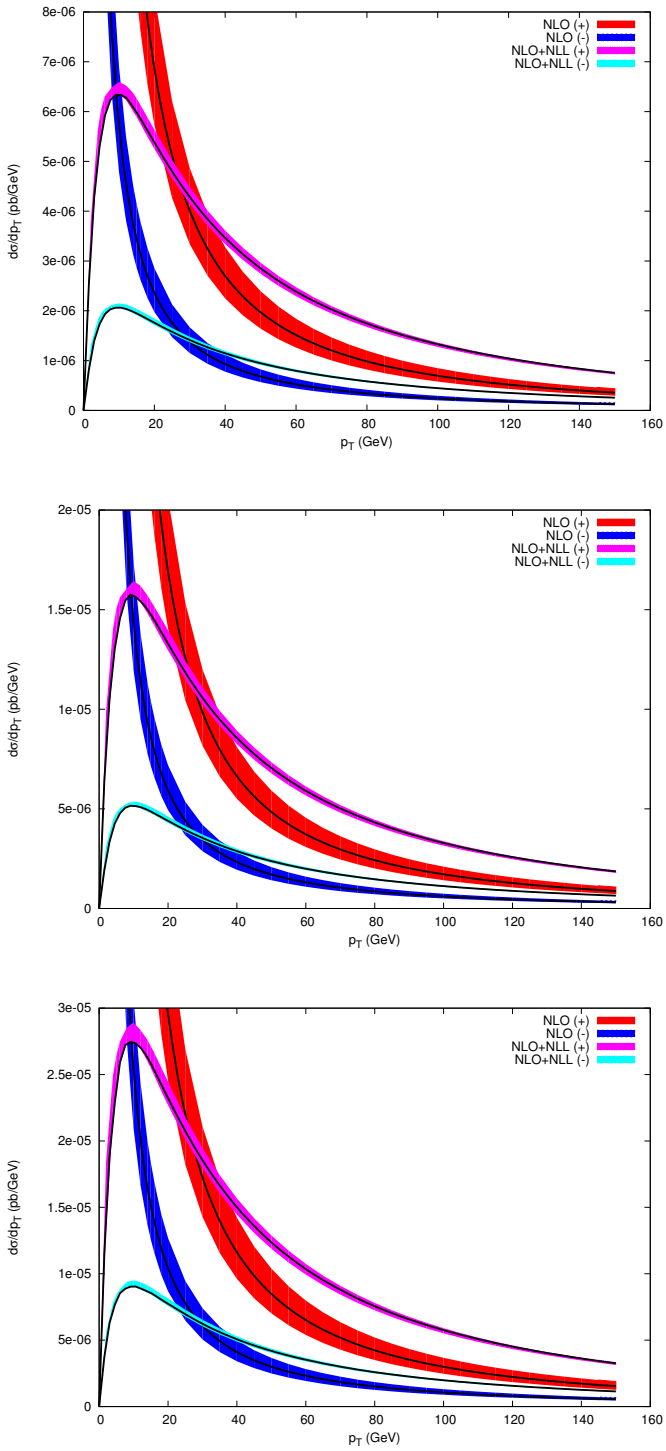

Figure 6.8: Transverse-momentum distribution for the production of $W'^{\pm}$ bosons of mass 4 TeV in a proton-proton collider at a center-of-mass-energy of 14 TeV in the UU model for parameter t of (from top to bottom) 0.4, 0.7 and 1.2. The rest of the parameters are the same as in Fig. 6.1.

6.3 The nonuniversal model

Table 6.3: Benchmark points and the corresponding total cross sections for $W'^{\pm}$ in the ununified model. The new gauge boson mass is 4 TeV and the center-of-mass energy is 14 TeV. The rest of parameters and the uncertainties are defined as in Tab. 6.1.

Boson	Mass	σ_{LO} (ab)	σ_{NLO} (ab)	σ_{res} (ab)
W'^{+}	0.7	$3511.1^{+496.2}_{-410.7}$	$3868.4^{+350.9+175.4}_{-328.5-116.7}$	$3780.9^{+311.8+655.0}_{-0.0-131.1}$
W'^{-}	0.7	$1035.0^{+144.8}_{-120.1}$	$1339.8^{+118.8+129.4}_{-108.7-53.8}$	$1433.0^{+34.2+303.1}_{-23.3-56.6}$
W'^{+}	1.2	$643.7^{+91.8}_{-75.9}$	$712.0^{+62.0+36.4}_{-58.6-22.4}$	$690.0^{+65.0+127.9}_{-0.0-25.5}$
W'^{-}	1.2	$189.3^{+26.7}_{-22.1}$	$249.2^{+21.3+23.8}_{-20.1-10.5}$	$266.6^{+5.5+58.0}_{-4.4-10.7}$
W'^{+}	1.4	$326.5^{+47.1}_{-39.0}$	$359.4^{+32.2+17.7}_{-28.2-10.7}$	$347.3^{+35.3+63.7}_{-0.0-11.8}$
W'^{-}	1.4	$96.5^{+13.7}_{-11.3}$	$125.9^{+10.8+12.8}_{-9.7-5.0}$	$135.0^{+3.0+30.3}_{-2.0-5.2}$

Finally we will show the results obtained for the nonuniversal (NU) model. For this model we have also shown the parametrization done in Ref. [48] in which the different models are defined by the new gauge boson mass $m_{Z'(W')}$ and a free parameter t. In this case the models with gauge boson masses of $m_{W'} \sim 3$ TeV are already ruled out, so we have focused on heavy gauge bosons with mass $m_{W'} = 4$ TeV at the design center-of-mass energy $\sqrt{S} = 14$ TeV. We have chosen, similarly to the UU case, three values for the parameter t in the allowed parameter space, namely $t \in \{0.7, 1.2, 1.4\}$. The values span as much as possible of the phenomenologically interesting region of the parameter space, while having some overlap with the previous UU models.

We have computed the total cross section at LO, NLO and threshold resummation matched to NLO. A summary of the chosen benchmark points and the corresponding results are shown in Tab. 6.3, together with the corresponding uncertainties. All the parameters and uncertainty analysis has been done as explained for the SSM. We also show the transverse-momentum distributions in the spirit of previous analyses in Fig. 6.9. For simplicity only scale uncertainties are shown in the distributions.

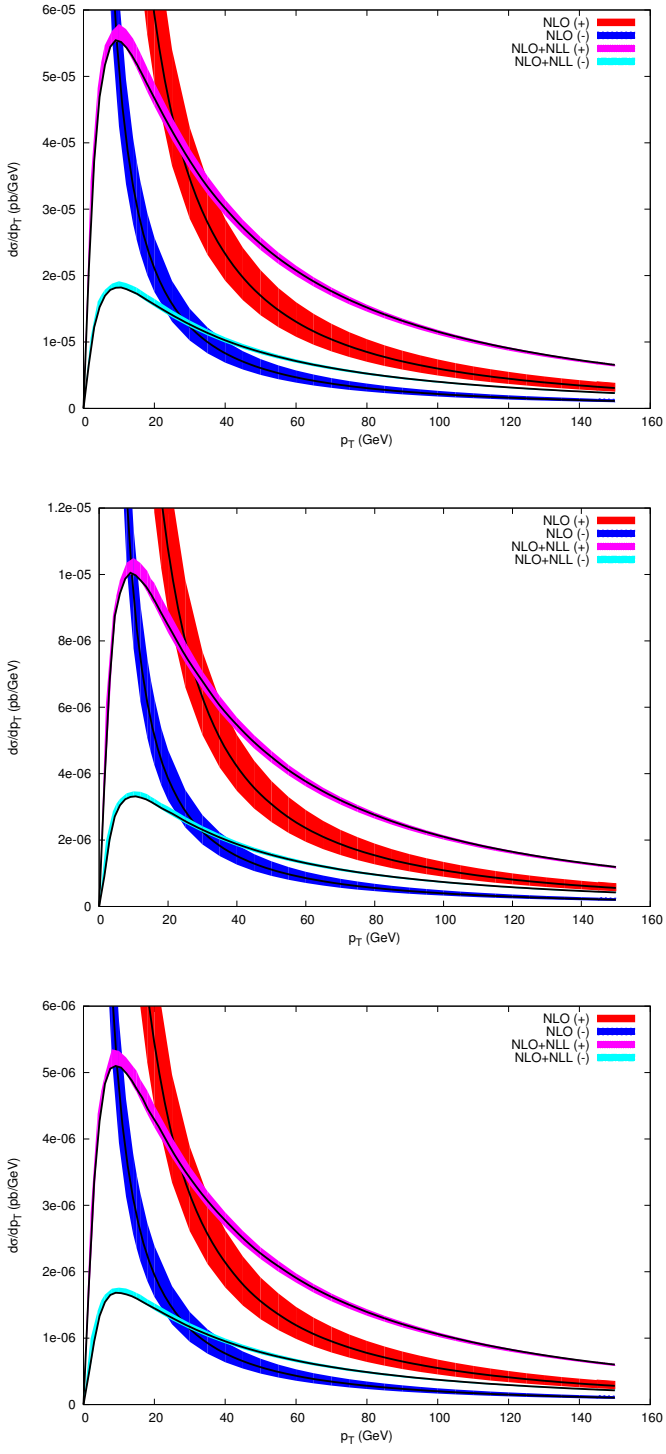

Figure 6.9: Transverse-momentum distribution for the production of $W'^{\pm}$ bosons of mass 4 TeV in a proton-proton collider at a center-of-mass-energy of 14 TeV in the NU model for parameter t of (from top to bottom) 0.7, 1.2 and 1.4. The rest of the parameters are the same as in Fig. 6.1.

Chapter 7

Conclusions

In this work we have investigated the production of new gauge bosons at proton-proton colliders, and the LHC in particular, including resummation corrections.

We have reviewed the concept of resummation and the necessary formulae for the application of the threshold and transverse-momentum formalisms in a Drell-Yan-like process.

After introducting some of the main theories that lead to the existence of new gauge bosons Z' and W' in a general phenomenological framework that allows comprehensive analysis of a wide range of theoretical possibilities, we have analytically computed fixed-order predictions at leading order and next-to-leading order in the strong coupling for the production of these new gauge bosons at hadron colliders.

We have then presented specific numerical predictions for some of the presented models by choosing benchmark points in the parameter space of each model. We have included predictions for total cross section and transverse-momentum distributions.

This work is, to our knowledge, the first application of resummation corrections to Z' production in non-GUT theories and the first application to W' bosons, having seen that in some models the cross sections for W' can be much larger than for Z' and therefore they could represent the discovery channel for new physics, and maybe even the only available at our accesible energies. The precision resummation predictions can be currently used to set precise limits on new gauge boson properties and could be used after a potential discovery to determine the properties of the new gauge bosons and to distinguish between the different theoretical possibilities.

Appendix A

Gaugino-pair production

Supersymmetry (or SUSY) is arguably the most important BSM theory. Its mathematical elegance and phenomenogical consequences make it one of the most studied models of particle physics. The discovery of a particle compatible with a light Higgs boson [1, 2] immediately raises the question of the so-called hierarchy problem, since it is known that fundamental scalar particles are affected by large quantum corrections. One of the most well-known solutions to this problem is supersymmetry. Furthermore, a number of other theoretical issues are also resolved in supersymmetry, like the Grand Unification of the different forces and the existence of a dark matter candidate. LHC SUSY searches have until now focused on strongly charged SUSY particles, but no signs of squarks or gluinos have yet been found [61]. Thus, the attention is shifted towards the electroweak channels. Moreover, an unexpected result from the CMS collaboration suggests that W^+W^- data fits theoretical predictions better when including gauginos in the analysis than with the SM alone [62]. These reasons motivate us to present up-to-date precision predictions for these electroweak channels.

In this chapter we present the basics of the work published in Ref. [10]. We will introduce the motivation and concept of supersymmetry, review the basics of the gaugino sector of the Minimal Supersymmetric Standard Model (MSSM) and explain and present the predictions done for gaugino production at the LHC, using the resummation formalisms presented in Ch. 3.

A.1 Motivation for supersymmetric theories

It is known that the underlying space-time symmetry of the S-matrix is the Poincaré symmetry group $\mathcal{P}$, given by

$$[P_\mu, P_\nu] = 0, \tag{A.1}$$
$$[P_\mu, M_{\nu\rho}] = i(g_{\mu\nu}P_\rho - g_{\mu\rho}P_\nu), \tag{A.2}$$
$$[M_{\mu\nu}, M_{\rho\sigma}] = i(g_{\mu\rho}M_{\nu\sigma} - g_{\mu\rho}M_{\nu\rho} + M_{\mu\rho}g_{\nu\sigma} - M_{\mu\rho}g_{\nu\rho}), \tag{A.3}$$

where $g_{\mu,\nu}$ is the Minkowski metric, P_μ is the energy-momentum operator and $M_{\mu\nu}$ are the generators of the angular momentum and boosts.

Coleman and mandule proved [63] that under certain conditions any Lie group that contains the Poincaré group must be a direct product $\mathcal{P} \times \mathcal{G}$ with $\mathcal{G}$ an internal symmetry group. Haag, Lopuszanski and Sohnius [64] noticed that by relaxing one of the conditions, i.e. by introducing anticommuting symmetry generators, there exists a unique non-trivial extension of the Poincaré algebra, given by

$$\{Q^i_\alpha, \bar{Q}^j_{\dot\beta}\} = 2(\sigma^\mu)_{\alpha\dot\beta}P_\mu\delta_{ij}, \tag{A.4}$$
$$\{Q^i_\alpha, Q^j_\beta\} = \epsilon_{\alpha\beta}Z^{ij}, \tag{A.5}$$
$$[Q^i_\alpha, P_\mu] = 0, \tag{A.6}$$
$$[Q^i_\alpha, M_{\mu\nu}] = i(\sigma_{\mu\nu})^\beta_\alpha Q^i_\beta, \tag{A.7}$$

where Q^i_α with $i \in \{1, \ldots, N\}$ are the SUSY generators and $Z^{ij} = -Z^{ji}$ are the so-called central charges (vanishing for $N = 1$ SUSY), $\epsilon_{\alpha\beta}$ an antisymmetris tensor with $\epsilon_{12} = 1$ and $\sigma^\mu, \bar\sigma^\mu, \sigma^{\mu\nu}$ defined by

$$(\sigma^\mu)_{\alpha\dot\alpha} := (I, \sigma_x, \sigma_y, \sigma_z)_{\alpha\dot\alpha}, \tag{A.8}$$
$$(\bar\sigma^\mu)^{\dot\alpha\alpha} := \epsilon^{\dot\alpha\dot\beta}\epsilon^{\alpha\beta}(\sigma^\mu)_{\beta\dot\beta}, \tag{A.9}$$
$$(\sigma^{\mu\nu})^\beta_\alpha := \frac{1}{4}(\sigma^\mu\bar\sigma^\nu - \sigma^\nu\bar\sigma^\mu)^\beta_\alpha, \tag{A.10}$$

where I is the identity matrix and $\sigma_{x,y,z}$ are the usual Pauli matrices.

The particles are in the irreducible representation of the defined superalgebra, in the form of multiplets, each of them containing the same number of bosonic and fermionic degrees of freedom. Thus, each particle of the SM has a corresponding superpartner, which is bosonic for SM fermions and fermionic for SM bosons. From the superalgebra, both SM particle and superpartner should have degenerate masses, and therefore the SUSY particles should have already been seen. This means that SUSY must be a broken symmetry. We will not enter into the details of the possible SUSY breaking schemes or will introduce the notation of superspace or superfields. For a more detailed and relatively up-to-date review the reader is referred to, e.g. Ref. [65].

A.2 Gauginos in the MSSM

The simplest model of a supersymmetric theory is the Wess-Zumino model [66] and the minimal phenomenological viable (although currently very constrained) model is the Minimal Supersymmetric Standard Model (MSSM) [67], which embeds both $N = 1$ SUSY and the SM. The MSSM has two supermultiplets: one chiral supermultiplet with a complex scalar field and a Weyl fermion, and one vector supermultiplet containing a Weyl fermion associated with a vector boson. The SM fermions are included in the chiral supermultiplet and get superpartners called squarks and sleptons for quarks and leptons respectively. To avoid anomalies, two Higgs doublets are needed in the MSSM, which are included in the chiral supermultiplet together with their superpartners, the higgsinos. The SM bosons are included into the vector supermultiplet with their superpartners, which are called gauginos. This is summarized in Tabs. A.1 and A.2.

Particles	Spin 0	Spin 1/2
Squarks and quarks	$\tilde{q} = (\tilde{u}_\mathrm{L}, \tilde{d}_\mathrm{L})$	$q_\mathrm{L} = (u_\mathrm{L}, d_\mathrm{L})$
	$\tilde{u}^\dagger_\mathrm{R}$	$u^\dagger_\mathrm{R}$
	$\tilde{d}^\dagger_\mathrm{R}$	$d^\dagger_\mathrm{R}$
Sleptons and leptons	$\tilde{l}_\mathrm{L} = (\tilde{\nu}_\mathrm{L}, \tilde{e}_\mathrm{L})$	$l_\mathrm{L} = (\nu_\mathrm{L}, e_\mathrm{L})$
	$\tilde{e}^\dagger_\mathrm{R}$	$e^\dagger_\mathrm{R}$
Higgiginos and Higgs	$h_1 = (H^0_1, H^-_1)$	$\tilde{h}_1 = (\tilde{H}^0_1, \tilde{H}^-_1)$
	$h_2 = (H^+_2, H^0_2)$	$\tilde{h}_2 = (\tilde{H}^+_2, \tilde{H}^0_2)$

Table A.1: Particles in the chiral supermultiplet of the MSSM.

The higgsinos and the electroweak gauginos mix in general with each other because of electroweak symmetry breaking. Thus, the neutral $\tilde{H}^0_{1,2}$ mix with the $\tilde{B}, \tilde{W}^0$ gauginos to form four neutral sparticles, the neutralinos, denoted by χ^0_i with $i \in \{1, 2, 3, 4\}$, such that $m_{\chi^0_i} < m_{\chi^0_j}$ iff $i < j$. The neutralino χ^0_1 is in often the lightest supersymmetric particle (LSP) and thus a dark matter candidate in R-conserving theories. On the other hand, the charged $\tilde{H}^{+(-)}_{1,2}$ mix with the winos $\tilde{W}^{+(-)}$ giving the mass eigenstate called chargino, and denoted by $\chi^{+(-)}_k$, with $k \in \{1, 2\}$ and $m_{\chi^{+(-)}_i} < m_{\chi^{+(-)}_j}$.

Particles	Spin 1/2	Spin 1
Gluinos and gluons	$\tilde{g}$	g
Winos and W bosons	$\tilde{W}^+, \tilde{W}^-, \tilde{W}^0$	W^+, W^-, W^0
Bino and B boson	$\tilde{B}$	B

Table A.2: Particles in the vector supermultiplet of the MSSM.

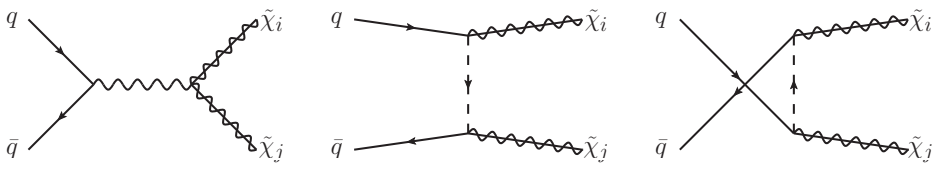

Figure A.1: Leading-order Feynman diagrams for gaugino production at hadron colliders. From Ref. [7].

The particular mixing depends on the parameters of the MSSM model, in particular on β, μ, which are related to the SUSY breaking (see Ref. [65] for the expressions for the mixing matrices).

A.3 Gaugino-pair production at hadron colliders

Since neutralinos and charginos contain a mixing with electroweak gauginos they inherit electroweak couplings. Thus, gauginos can be produced in a hadron collider through an s-channel in the decay of an electroweak gauge boson Z to two neutralinos or two charginos of opposite electrical charge, or the decay of a charged $W^{+(-)}$ to a chargino-neutralino pair, similarly to the Drell-Yan-like processes previously studied. In addition, they can be produced through $t-$ and $u-$channels by the exchange of a squark (the superpartner of the quark). The computations for the corresponding cross sections up to next-to-leading order matched with resummation can be found in Refs. [7, 8] and references therein. The LO contributions are depicted in Fig. A.1 for reference, and the NLO diagrams as well as the full analytical computations can be found in Ref. [7].

A.4 Numerical results

We have updated the resummation predictions for gaugino-pair production for SUSY searches at the LHC. The full set of results can be found in Ref. [10], but we will show here only some examples in a similar fashion to those presented in Ch. 6.

The first issue when making numerical predictions for a SUSY model is to determine the set of parameters to use. Original MSSM has a total of 124 parameters, that can be reduced to five in the contrained MSSM (cMSSM). The LHC experimental collaborations have chosen a set of 49 benchmark points in different lines of the parameter space for USY discussions. We selected thirteen out of these defined points lying on different lines. In particular for further analyses we focused on one point of each line, namely points 1, 18 and 31 in the LPCC numbering scheme. A more detailed discussion and references can be found in Ref. [10].

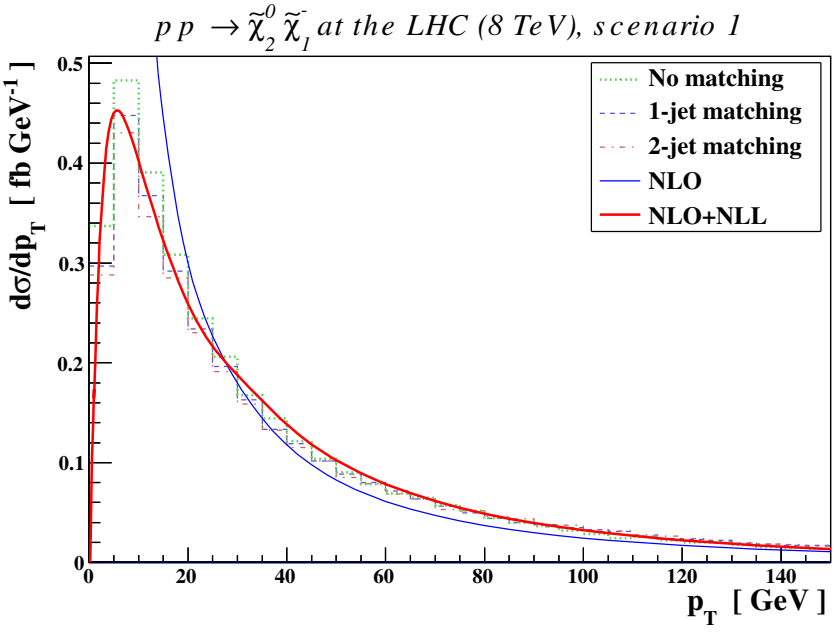

Figure A.2: Transverse momentum (p_{T}) distribution for the production of $\chi_2^0\chi_1^-$ in proton-proton collisions at a center-of-mass energy of 8 TeV for benchmark point 1 of the LPCC. Next-to-leading order, next-to-leading order matched with resummation, and results from Monte Carlo generators matched to 1 and 2 jets are shown. See Ref. [10] for more details.

Here we will show the cross sections obtained for the benchmark point 1 of the LPCC, for proton-proton collisions at a center-of-mass energy of 8 TeV. We have used MSTW 2008 NLO PDF as the parton distribution function and have set the scales $\mu_{\mathrm{F}} = \mu_{\mathrm{R}} = \mu$ to the average final state particle mass and varied them multipying the central value by a factor in the range $[0.5, 2]$. The results are shown in Tab. A.3. We can see that the production of $\chi_2^0\chi_1^-$, the so-called golden channel, as well as $\chi_1^+\chi_1^-$ are clearly enhanced. This is a common feature to many SUSY models, where the χ_1^0 is mostly bino. This is due to the fact that the given pairs have large couplings to the SM bosons as well as kinematical effects [65].

Finally we present in Fig. A.2 a transverse momentum (p_{T}) distribution similarly to the ones given in Ch. 6. Additionally we include results from Monte Carlo generators, which are commonly used by experimental collaborations. We can see that NLO results are clearly unstable and that resummation fits quite well with results from simulations. The best fit is the 1-jet matching since we include a single (hard) jet in out NLO and NLO+NLL computations.

Channel	m_1 (TeV)	m_2 (TeV)	LO (fb)	NLO (fb)	NLO+NLL (fb)
$\chi_1^0\chi_1^0$	161.7	161.7	$0.81^{+5.8\%}_{-5.3\%}$	$1.06^{+3.5\%+2.8\%}_{-3.0\%-2.0\%}$	$1.03^{+0.5\%+2.9\%}_{-0.6\%-2.0\%}$
$\chi_1^0\chi_1^-$	161.7	303.5	$0.16^{+6.0\%}_{-5.5\%}$	$0.20^{+2.5\%+2.9\%}_{-2.4\%-2.4\%}$	$0.20^{+0.0\%+2.9\%}_{-0.3\%-2.5\%}$
$\chi_2^0\chi_2^0$	303.8	303.8	$0.85^{+9.2\%}_{-7.9\%}$	$1.07^{+3.5\%+3.1\%}_{-3.5\%-2.2\%}$	$1.05^{+0.0\%+3.5\%}_{-0.4\%-1.9\%}$
$\chi_2^0\chi_3^0$	303.8	526.5	$0.21^{+9.4\%}_{-8.1\%}$	$0.25^{+2.6\%+3.2\%}_{-2.9\%-2.3\%}$	$0.25^{+0.1\%+3.2\%}_{-0.5\%-2.3\%}$
$\chi_2^0\chi_1^-$	303.8	303.5	$14.46^{+6.7\%}_{-6.1\%}$	$17.25^{+1.6\%+3.0\%}_{-1.7\%-2.6\%}$	$17.05^{+0.2\%+3.1\%}_{-0.7\%-2.6\%}$
$\chi_3^0\chi_4^0$	526.5	542.4	$0.83^{+11.0\%}_{-9.3\%}$	$0.97^{+2.8\%+3.9\%}_{-3.3\%-2.4\%}$	$0.96^{+0.4\%+3.8\%}_{-0.9\%-2.5\%}$
$\chi_3^0\chi_1^-$	526.5	303.5	$0.12^{+9.4\%}_{-8.1\%}$	$0.15^{+2.6\%+3.8\%}_{-2.9\%-2.9\%}$	$0.15^{+0.1\%+3.8\%}_{-0.6\%-3.0\%}$
$\chi_3^0\chi_2^-$	526.5	542.2	$0.42^{+11.2\%}_{-9.5\%}$	$0.50^{+2.8\%+4.9\%}_{-3.3\%-3.6\%}$	$0.49^{+0.4\%+4.9\%}_{-0.9\%-3.5\%}$
$\chi_4^0\chi_2^-$	542.4	542.2	$0.39^{+11.3\%}_{-9.6\%}$	$0.47^{+2.7\%+4.9\%}_{-3.2\%-3.6\%}$	$0.46^{+0.5\%+4.9\%}_{-1.1\%-3.7\%}$
$\chi_1^+\chi_1^0$	303.5	161.7	$0.38^{+6.0\%}_{-5.4\%}$	$0.46^{+2.5\%+2.8\%}_{-2.4\%-2.1\%}$	$0.46^{+0.2\%+2.9\%}_{-0.5\%-2.1\%}$
$\chi_1^+\chi_2^0$	303.5	303.8	$35.16^{+6.3\%}_{-5.8\%}$	$40.90^{+1.6\%+2.9\%}_{-1.7\%-2.2\%}$	$40.51^{+0.0\%+2.9\%}_{-0.3\%-2.2\%}$
$\chi_1^+\chi_3^0$	303.5	526.5	$0.34^{+9.2\%}_{-7.9\%}$	$0.40^{+2.6\%+3.7\%}_{-2.9\%-2.4\%}$	$0.40^{+0.0\%+3.6\%}_{-0.3\%-2.5\%}$
$\chi_1^+\chi_1^-$	303.5	303.5	$25.64^{+6.6\%}_{-5.9\%}$	$30.37^{+1.7\%+2.7\%}_{-1.9\%-2.0\%}$	$30.04^{+0.0\%+2.7\%}_{-0.5\%-2.1\%}$
$\chi_2^+\chi_3^0$	542.2	526.5	$1.27^{+11.1\%}_{-9.4\%}$	$1.46^{+2.9\%+4.4\%}_{-3.3\%-2.7\%}$	$1.45^{+0.3\%+4.3\%}_{-0.7\%-2.9\%}$
$\chi_2^+\chi_4^0$	542.2	542.4	$1.21^{+11.2\%}_{-9.5\%}$	$1.37^{+2.7\%+4.4\%}_{-3.2\%-2.8\%}$	$1.36^{+0.4\%+4.6\%}_{-0.8\%-2.6\%}$
$\chi_2^+\chi_2^-$	542.2	542.2	$0.86^{+10.9\%}_{-9.3\%}$	$1.00^{+2.6\%+4.0\%}_{-3.1\%-2.4\%}$	$0.99^{+0.4\%+4.1\%}_{-0.9\%-2.4\%}$

Table A.3: Total cross section for gaugino-pair production of masses m_i at leading order, next-to-leading order and next-to-leading order matched with resummation in proton-proton collisions at a center-of-mass energy of 8 TeV for benchmark poin 1 of the LPCC. The first error is due to scale variation $\mu_F/M = \mu_R/M = \mu_F/M \in \{0.5, 1, 2\}$ and the second to MSTW 2008 NLO PDF error.

Acknowledgements

I would like to express my gratitude to the following people:

- Prof. Dr. Michael Klasen, for giving me the opportunity to work in this exciting world and for all the things he taught me.
- Prof. Dr. Juan A. Caballero and Prof. Dr. Manuel Morillo, for their help and support during this year.
- Prof. Dr. Benjamin Fuks, for his patience to teach me.
- Marcel Rothering and the rest of the group for creating such a nice atmosphere.
- Dra. Carmen Lozano and Dr. Julio Carmona for the many things they taught me.
- Dr. Francisco Martínez-Cuadrado and the "Sacrocoro," for so many hours of interesting discussions, sometimes even about literature.
- My friends Francisco J. Morales and Jose Á. Rufino, for many things.
- Ariadna Corral, for everything we shared, and especially for everything yet to come.
- My grandparents Rocio Morales and Antonio Lamprea, my father Luis Regalado, my stepmother Margarita Delgado, my brother Luis Regalado, and especially my sister, Margarita Regalado, for their continuous love and support.

Abschlusserklärung

Ich versichere hiermit, dass ich meine Master-Abschlussarbeit selbstständig und ohne fremde Hilfe angefertigt habe, und dass ich alle von anderen Autoren wörtlich übernommenen Stellen wie auch die sich an die Gedankengänge anderer Autoren eng anlehnenden Ausführungen meiner Arbeit besonders gekennzeichnet und die Quellen zitiert habe.

Münster, den Oktober 2012.

Bibliography

[1] The ATLAS Collaboration, Phys. Lett. B **716**, 1 (2012).

[2] The CMS Collaboration, Phys. Lett. B **716**, 30 (2012).

[3] G. Sterman, Nucl. Phys. B **281**, 310 (1987).

[4] A. Kulesza and L. Motyka, Phys. Rev. Lett. **102**, 111802 (2009).

[5] A. Kulesza and L. Motyka, Phys. Rev. D **80**, 095004 (2009).

[6] W. Beenakker, S. Brensing, M. Krämer, A. Kulesza, E. Laenen, and I. Niessen, JHEP **12**, 041 (2009).

[7] J. Debove, B. Fuks, and M. Klasen, Nucl. Phys. B **842**, 51 (2011).

[8] J. Debove, B. Fuks, and M. Klasen, Phys. Lett B **688**, 208 (2010).

[9] J. Debove, B. Fuks, and M. Klasen, Nucl. Phys. B **849**, 64 (2011).

[10] B. Fuks, M. Klasen, D. R. Lamprea, and M. Rothering, JHEP **10**, 081 (2012).

[11] B. Fuks, M. Klasen, F. Ledroit, Q. Li, and J. Morel, Nucl. Phys. B **797**, 322 (2008).

[12] J. C. Collins and D. E. Soper, Ann. Rev. Nucl. Part. Sci. **37**, 383 (1987).

[13] T. Plehn, arXiv:0910.4182 [hep-ph].

[14] A. D. Martin, W. J. Stirling, R. S. Thorne, and G. Watt, Eur. Phys. J. C **63**, 189 (2009).

[15] S. Drell and T. Yan, Phys. Rev. Lett. **25**, 316 (1970).

[16] R. K. Ellis, W. J. Stirling, and B. R. Webber, *QCD and Collider Physics* (Cambridge University Press, 1996).

[17] G. Passarino and M. J. G. Veltman, Nucl. Phys. B **160**, 151 (1979).

[18] G. Sterman, arXiv:hep-ph/9606312.

[19] E. Laenen, Pramana **63**, 1225 (2004).

[20] J. Debove, Ph.D. thesis, Université de Grenoble (2011).

[21] G. Bozzi, B. Fuks, and M. Klasen, Nucl. Phys. B **777**, 157 (2007).

[22] G. Bozzi, B. Fuks, and M. Klasen, Phys. Rev. D **74**, 015001 (2006).

[23] B. Fuks, Ph.D. thesis, Université Joseph Fourier (2011).

[24] T. Kinoshita, J. Math. Phys. **3**, 650 (1962).

[25] T. D. Lee and M. Nauenberg, Phys. Rev. B **133**, 1549 (1964).

[26] G. Altarelli and G. Parisi, Nucl. Phys. B **126**, 298 (1977).

[27] S. Catani and L. Trentadue, Nucl. Phys. B **327**, 323 (1989).

[28] J. C. Collins, D. Soper, and G. Sterman, Nucl. Phys. B **250**, 199 (1985).

[29] S. Catani, D. de Florian, and M. Grazzini, Nucl. Phys. B **596**, 299 (2001).

[30] D. de Florian and M. Grazzini, Phys. Rev. Lett. **85**, 4678 (2000).

[31] D. de Florian and M. Grazzini, Nucl. Phys. B **616**, 247 (2001).

[32] J. Beringer et al. (Particle Data Group), Phys. Rev. D **86**, 010001 (2012).

[33] G. Altarelli, B. Mele, and M. Ruiz-Altaba, Z. Phys. C **45**, 109 (1989).

[34] The CMS Collaboration, arXiv:1204.4764 [hep-ex].

[35] H. Georgi and S. Glashow, Phys. Rev. Lett. **32**, 438 (1974).

[36] H. Georgi, H. Quinn, and S. Weinberg, Phys. Rev. Lett. **33**, 451 (1974).

[37] J. L. Hewett and T. G. Rizzo, Phys. Rep. **5**, 19 (1989).

[38] S. Nie and M. Sher, arXiv:hep-ph/0102139.

[39] A. Leike, arXiv:hep-ph/9805494.

[40] J. Erler, O. Langacker, S. Munir, and E. Rojas, arXiv:0906.2435 [hep-ph].

[41] R. N. Mohapatra and J. C. Pati, Phys. Rev. D **11**, 566 (1975).

[42] R. N. Mohapatra and J. C. Pati, Phys. Rev. D **11**, 2558 (1975).

[43] R. N. Mohapatra and G. Senjanovic, Phys. Rev. D **23**, 165 (1981).

[44] K. Hsieh, K. Schmitz, J.-H. Yu, and C.-P. Yuan, Phys. Rev. D **82**, 035011 (2012).

[45] H. Georgi, E. E. Jenkins, and E. H. Simmons, Phys. Rev. Lett. **62**, 2789 (1989).

[46] E. Malwaki, T. M. P. Tait, and C.-P. Yuan, Phys. Lett. B **385**, 304 (1996).

[47] P. Langacker and S. U. Sankar, Phys. Rev. D **40**, 1569 (1989).

[48] T. Jezo, Master's thesis, Université Joseph Fourier (2009).

[49] G. Rizzo, arXiv:hep-ph/0105239.

[50] P. Osland et al., Phys. Rev. D **79**, 115021 (2009).

[51] The CMS Collaboration, J. Phys. G **34**, 995 (2007).

[52] The CMS Collaboration, arXiv:1206.1849 [hep-ex].

[53] The ATLAS Collaboration, ATLAS-CONF-2012-129.

[54] The CMS Collaboration, arXiv:1206.3921 [hep-ex].

[55] The ATLAS Collaboration, ATLAS-CONF-2012-086.

[56] The CMS Collaboration, CMS PAS EXO-12-010.

[57] B. Pötter, INSPIRE-1185169.

[58] M. Böhm, A. Denner, and H. Joos, *Gauge Theories of the Strong and Electroweak Interaction* (Teubner, 2001).

[59] G. 't Hooft and M. Veltmann, Nucl. Phys. B **44**, 189 (1972).

[60] J. A. M. Vermaseren, arXiv:math-ph/0010025.

[61] The CMS Collaboration, arXiv:1205.4053 [hep-ex].

[62] The CMS Collaboration, arXiv:1206.6888 [hep-ex].

[63] S. R. Coleman and J. Mandula, Phys Rev. **159**, 1251 (1967).

[64] R. Haag, J. T. Lopuszanski, and M. Sohnius, Nucl. Phys. B **88**, 257 (1975).

[65] S. P. Martin, arXiv:hep-ph/9709356.

[66] J. Wess and B. Zumino, Nucl. Phys. B **70**, 39 (1974).

[67] J. Wess and B. Zumino, Nucl. Phys. B **78**, 52 (1974).